BIOCHEMISTRY

Inhibition of ACLY overcomes cancer immunotherapy resistance via polyunsaturated fatty acids peroxidation and cGAS-STING activation

Wei Xiang[1]†, Hongwei Lv[1,2,3]†, Fuxue Xing[1]†, Xiaoyan Sun[4]†, Yue Ma[1], Lu Wu[5], Guishuai Lv[2,3], Qianni Zong[2,3], Liang Wang[2,3], Zixin Wu[1], Qiyu Feng[1], Wen Yang[1,2,3,6,7]*, Hongyang Wang[1,2,3,4,6,7]*

Adenosine 5′-triphosphate citrate lyase (ACLY) is a cytosolic enzyme that converts citrate into acetyl–coenzyme A for fatty acid and cholesterol biosynthesis. ACLY is up-regulated or activated in many cancers, and targeting ACLY by inhibitors holds promise as potential cancer therapy. However, the role of ACLY in cancer immunity regulation remains poorly understood. Here, we show that ACLY inhibition up-regulates PD-L1 immune checkpoint expression in cancer cells and induces T cell dysfunction to drive immunosuppression and compromise its antitumor effect in immunocompetent mice. Mechanistically, ACLY inhibition causes polyunsaturated fatty acid (PUFA) peroxidation and mitochondrial damage, which triggers mitochondrial DNA leakage to activate the cGAS-STING innate immune pathway. Pharmacological and genetic inhibition of ACLY overcomes cancer resistance to anti–PD-L1 therapy in a cGAS-dependent manner. Furthermore, dietary PUFA supplementation mirrors the enhanced efficacy of PD-L1 blockade by ACLY inhibition. These findings reveal an immunomodulatory role of ACLY and provide combinatorial strategies to overcome immunotherapy resistance in tumors.

INTRODUCTION

Currently, immune checkpoint blockade has achieved tremendous clinical breakthroughs in cancer immunotherapy (1–3). Programmed death ligand 1 (PD-L1) is abundantly expressed in various tumors and has immunoregulatory function by dampening the immune response when bound to its receptor programmed cell death 1 (PD-1) on activated T cells (4). Blockade of the PD-1/PD-L1 axis markedly enhances T cell response and has exhibited dramatic antitumor efficacy in various types of advanced cancers (1–3). Unfortunately, the sustained benefit of PD-1/PD-L1 immune checkpoint blockade has been limited to approximately 20% of all malignancies presumably due to inadequate immune activation and there is increasing evidence of primary and adaptive resistance to immune checkpoint blockade in multiple cancer types (5, 6). Therefore, extensive efforts are underway to develop novel therapeutic strategies to potentiate immunotherapy efficacy and overcome immunotherapy resistance (7). Growing pieces of evidence have shown that cancer cell metabolism plays a crucial role in the regulation of antitumor immune response (8, 9). We have also recently demonstrated that nicotinamide adenine dinucleotide

(NAD⁺) metabolism drives tumor immune evasion and NAD⁺ replenishment sensitizes anti–PD-(L)1 [αPD-(L)1] therapy-resistant tumors to immunotherapy (10).

Enhanced lipid synthesis is among the most prominent metabolic hallmarks of cancer (11, 12). Adenosine 5′-triphosphate citrate lyase (ACLY) is a cytosolic enzyme that converts mitochondria-derived citrate into acetyl–coenzyme A (CoA), which is a precursor for de novo biosynthesis of fatty acids and cholesterol and is also required for acetylation reactions that modify proteins (13). ACLY is highly expressed in several types of cancers, supporting proliferation and maintaining stemness, and making this enzyme an attractive target for the treatment of cancer (14–17). ACLY has the advantage of being upstream of other lipogenic enzymes, and therefore, it is the preferential target to block de novo lipogenesis. ACLY inhibitors, previously developed for metabolic disorders, have recently drawn great interest as promising anticancer agents (13). In particular, bempedoic acid (BemA; also named ETC-1002) has been recently approved by U.S. Food and Drug Administration (FDA) for lowering low-density lipoprotein cholesterol (18). Although ACLY inhibition has been shown to inhibit cancer cell proliferation, the role of ACLY inhibition in tumor immunity and immunotherapy efficacy remains poorly understood.

cGMP-AMP (cGAMP) synthase (cGAS) is a cytosolic DNA sensor that activates innate immune responses (19, 20). Aberrant cytoplasmic DNA accumulation or cytosolic leakage of self-DNA is detected by cGAS, which catalyzes the synthesis of the second messenger cGAMP that binds and directly activates its downstream target, stimulator of interferon genes (STING) (19, 20). STING then activates TANK-binding kinase 1 (TBK1) to phosphorylate and activate interferon regulatory factor 3 (IRF3), which further induces the production of type I interferons (IFNs) and IFN-stimulated genes (ISGs) to promote cytotoxic T cell recruitment into tumors (21). cGAS-STING agonists are therefore being developed as a

[1]Cancer Research Center, First Affiliated Hospital of USTC, Division of Life Sciences and Medicine, University of Science and Technology of China, Hefei, Anhui 230027, China. [2]International Co-operation Laboratory on Signal Transduction, Eastern Hepatobiliary Surgery Institute/Hospital, Naval Medical University (Second Military Medical University), Shanghai 200438, China. [3]National Center for Liver Cancer, Naval Medical University (Second Military Medical University), Shanghai 201805, China. [4]First Affiliated Hospital of Zhengzhou University, Zhengzhou, Henan 450000, China. [5]Fourth Department of Hepatic Surgery, Eastern Hepatobiliary Surgery Hospital, Naval Medical University (Second Military Medical University), Shanghai 200438, China. [6]Shanghai Key Laboratory of Hepatobiliary Tumor Biology, Shanghai 200438, China. [7]Key Laboratory of Signaling Regulation and Targeting Therapy of Liver Cancer, Ministry of Education, Shanghai 200438, China.
*Corresponding author. Email: hywangk@vip.sina.com (H.W.); woodeasy66@hotmail.com (W.Y.)
†These authors contributed equally to this work.

promising cancer therapeutic (*22*, *23*). However, cGAS-STING agonist monotherapy has encountered profound cancer resistance in clinical trials (*22*, *23*).

Emerging evidence has demonstrated that the regulation of tumor immunity by the cGAS-STING pathway is dichotomous (*21*, *24*). For instance, cGAS-STING activation has been shown to drive immune evasion and metastasis by up-regulating the expression of PD-L1 on the surface of cancer cells (*25*). Thus, pharmacological activation of cGAS-STING alone may carry the side effect of immunosuppression. Nevertheless, tumor PD-L1 expression is a widely used and accepted biomarker of response to immune checkpoint inhibitors (*26*). Therefore, combined cGAS-STING agonists with immune checkpoint blockade can mechanistically synergize to repress tumor progression. In preclinical cancer models and clinical trials, the combination of cGAS-STING agonists and immune checkpoint blockade has achieved strong and durable efficacy (*27*, *28*).

In the current study, we discover that inhibition of ACLY leads to immunosuppression and compromises its antitumor effect in immunocompetent mice by polyunsaturated fatty acid (PUFA) peroxidation–induced cGAS-STING activation and PD-L1 up-regulation. Moreover, low ACLY expression correlates with cGAS-STING activation and exhausted T cell infiltration in human cancers. We further show that ACLY inhibition overcomes cancer resistance to αPD-L1 therapy in a cGAS-dependent manner and dietary PUFA supplementation is sufficient to mimic the enhanced efficacy of PD-L1 blockade by ACLY inhibition, providing promising combinational strategies for immunotherapy-resistant tumors therapy.

RESULTS
ACLY inhibition up-regulates PD-L1 expression in cancer cells and induces T cell dysfunction
To interrogate specific functions of ACLY, we disrupted Acly in wild-type murine liver cancer cells (Hepa1-6) by short hairpin–mediated RNA interference (shAcly). A reduction in ACLY was confirmed at the protein level (fig. S1A). In addition, BemA, an FDA-approved low-density lipoprotein cholesterol-lowering agent, was used to block the Acly enzyme activity of Hepa1-6 cells with high expression of very long-chain acyl-CoA synthetase 1 (ACSVL1) (fig. S1B), which is the enzyme that activates the BemA prodrug to bempedoyl-CoA, lastly inhibiting ACLY (*18*). To investigate the role of ACLY in tumor immunity, Acly-deficient cells or control cells were inoculated subcutaneously into the flanks of immunodeficient mice and immunocompetent mice, respectively. As expected, Acly deficiency significantly inhibited tumor growth in nude mice (Fig. 1, A and B, and fig. S1, C and D), consistent with previous reports (*14*, *15*). Unexpectedly, shAcly cell and shCtrl cells developed comparable-sized tumors in immunocompetent C57BL/6 mice (Fig. 1, A and B, and fig. S1, C and D). Similar results were observed when tumor ACLY was inhibited by BemA (fig. S1, E and F). Consistent with the observations made in nude mice, a notable inherent delay in tumor proliferation was observed in C57BL/6 mice (fig. S1G). These data indicate that the comparatively faster growth of Acly-deficient tumors in immunocompetent C57BL/6 mice, as compared to nude mice, can be attributed to the immunosuppressive effects resulting from ACLY inhibition.

To further investigate the mechanism of immunosuppression mediated by ACLY inhibition, we analyzed the correlation between ACLY and T cell–related immune checkpoint molecule expression in a dataset of human hepatocellular carcinoma (HCC), the most common type of liver cancer (*29*), and a significant negative correlation between ACLY and PD-L1 was observed (Fig. 1C). PD-L1 expression in Acly-deficient tumors was significantly higher than that in control tumors (Fig. 1D and fig. S1H), accompanied by increased infiltration of exhausted CD8$^+$ T cells with high PD-1 expression (Fig. 1, E and F). In addition, up-regulation of PD-L1 in cancer cells after ACLY inhibition was further confirmed at both transcriptional and protein levels by in vitro studies (fig. S1, I to L). In contrast, no significant changes of major histocompatibility complex class I expressions were observed in shAcly cells versus shCtrl cells, suggesting that ACLY loss of tumor cells had little effect on antigen presentation in our models (fig. S1M).

To further clarify the role of ACLY in tumor immunity, we compared the growth of murine pancreatic cancer cells (Pan02) with Acly knockdown in culture versus immunocompetent mice. Acly deficiency markedly repressed cancer cell proliferation in vitro (Fig. 1, G and H) but had no obvious difference in tumor growth in C57BL/6 mice (Fig. 1, I and J, and fig. S1, N and O), further confirming the immunosuppressive effect of ACLY inhibition compromising its antitumor effect in pancreatic cancer. Similar to liver cancer, ACLY expression was negatively correlated with PD-L1 immune checkpoint in the human pancreatic ductal adenocarcinoma (PDAC) dataset (Fig. 1K). Furthermore, compared with control tumors, shAcly tumors displayed increased PD-L1 expression (Fig. 1L) and T cell dysfunction, as shown by increased infiltration of exhausted CD8$^+$ T cells with high PD-1 expression and impaired function of CD8$^+$ T cells to secrete IFN-γ and granzyme B (GZMB) (Fig. 1, M to Q). The representative gating strategy used for flow cytometry analysis was shown in fig. S1P. Therefore, these results imply that ACLY inhibition up-regulates PD-L1 expression in cancer cells and induces T cell dysfunction.

ACLY inhibition leads to cGAS-STING activation
We next investigated the mechanism involved in ACLY inhibition–mediated up-regulation of PD-L1 and T cell dysfunction. Gene set enrichment analysis (GESA) [Kyoto Encyclopedia of Genes and Genomes (KEGG) pathway analysis] in pancreatic cancer from The Cancer Genome Atlas (TCGA) showed that ACLY was highly and negatively interrelated with cytoplasmic DNA sensing signaling (Fig. 2A). Similarly, Acly-deficient cells exhibited a notable enrichment of genes associated with cytoplasmic DNA sensing signaling (Fig. 2B). As a classic cytoplasmic DNA sensing signaling pathway, the cGAS-STING pathway is known to play a key role in tumor immunity by regulating PD-L1 expression in tumor cells and recruiting T cells (*21*). We further explored whether ACLY inhibition activated cGAS-STING signaling and found that ACLY knockdown up-regulated cGAS expression and induced downstream Sting signaling activation in Pan02, B16, and Hepa1-6 cells, as evidenced by the phosphorylation of Sting, Tbk1, and Irf3 proteins (Fig. 2, C and D). Similarly to ACLY deficiency, ACLY inhibitor BemA treatment effectively inhibited ACLY activity in Hepa1-6 cells in vitro and further led to cGAS-STING signaling activation, as evidenced by increases in p-Sting and p-Irf3 protein levels (Fig. 2, E and F),

It is known that cGAS activates downstream STING by producing cGAMP (*19*, *20*). As shown in Fig. 2G, more cGAMP
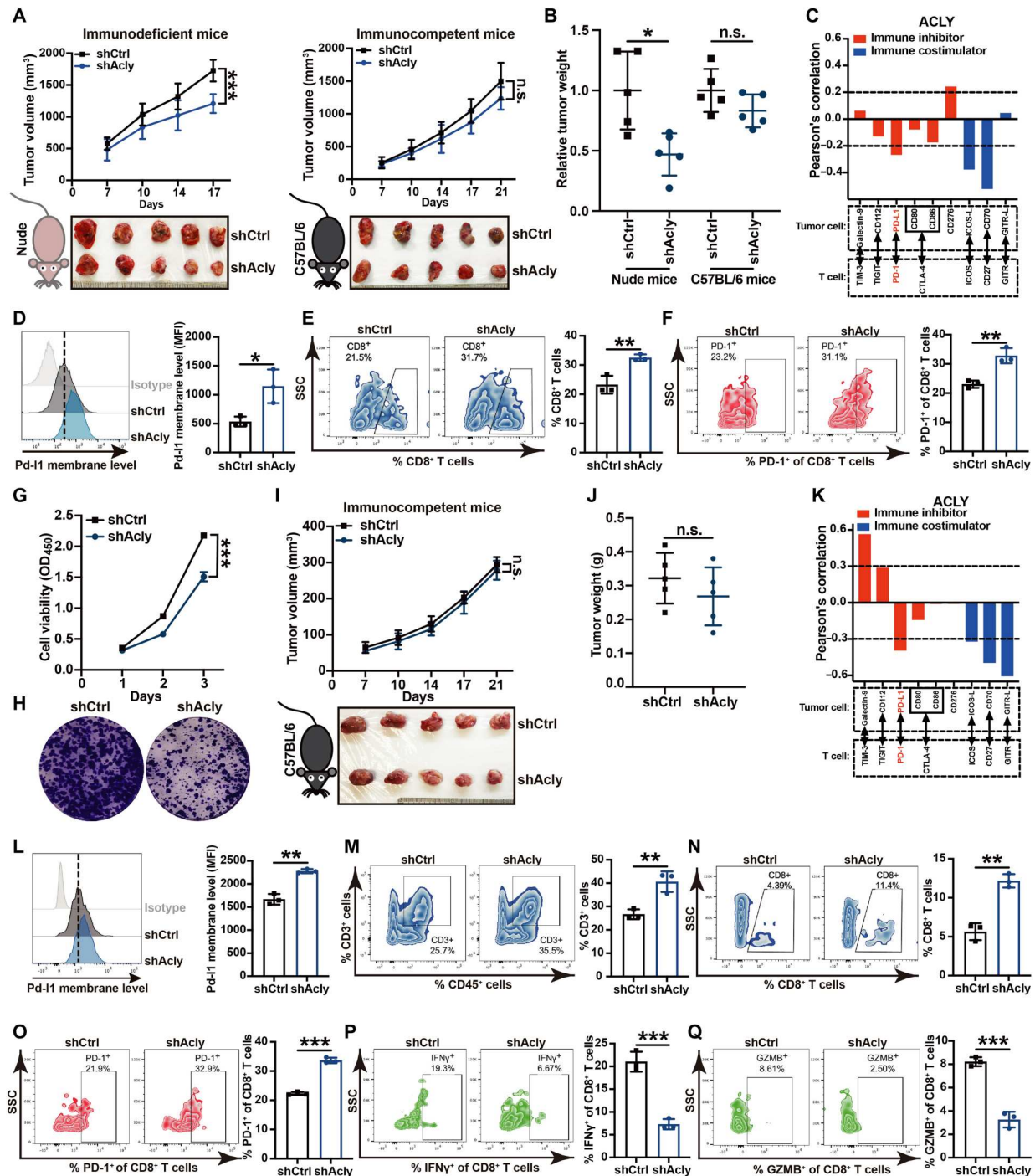
Fig. 1. ACLY inhibition up-regulates PD-L1 expression in cancer cells and induces T cell dysfunction. (**A** and **B**) Tumor growth (A) and relative tumor burdens (B) in immunodeficient nude mice and immunocompetent C57BL/6 mice injected subcutaneously with shAcly or shCtrl Hepa1-6 cells for 2 to 3 weeks. One additional independent experiment was performed that yielded similar results [fig. S1, (C) and (D)]. (**C**) Pearson's correlation between ACLY and T cell immune checkpoint molecules in human hepatocellular carcinoma (HCC) dataset (GSE45436) (*n* = 134 patients). (**D**) Flow staining and mean fluorescence intensity (MFI) of surface Pd-l1 of CD45⁻ cells in indicated Hepa1-6 tumors. (**E** and **F**) Flow staining and frequency of indicated cells in indicated Hepa1-6 tumors. (**G** and **H**) CCK-8 (G) and plate colony formation assay (H) for assessing the cell proliferation of shAcly or shCtrl Pan02 cells. (**I** and **J**) Tumor growth (I) and tumor burdens (J) in C57BL/6 mice injected subcutaneously with shAcly or shCtrl Pan02 cells for 3 weeks. One additional independent experiment was performed that yielded similar results [fig. S1, (N) and (O)]. (**K**) Pearson's correlation between ACLY and T cell immune checkpoint molecules in human PDAC dataset (GSE184585) (*n* = 82 patients). (**L**) Flow staining and MFI of surface Pd-l1 of CD45⁻ cells in indicated Pan02 tumors. (**M** to **Q**) Flow staining and frequency of indicated cells in indicated Pan02 tumors. *n* = 5 mice per group from one independent experiment [(A), (B), (I), and (J)]; *n* = 3 biological replicates from one independent experiment [(D) to (F) and (L) to (Q)]; *n* = 5 biological replicates from one independent experiment (G). Statistical significance was assessed by two-way analysis of variance (ANOVA) [(A), (G), and (I)] and unpaired *t* test [(B), (D) to (F), (J), and (L) to (Q)]; *P < 0.05; **P < 0.01; ***P < 0.001; n. s., not significant; OD₄₅₀, optical density at 450 nm.

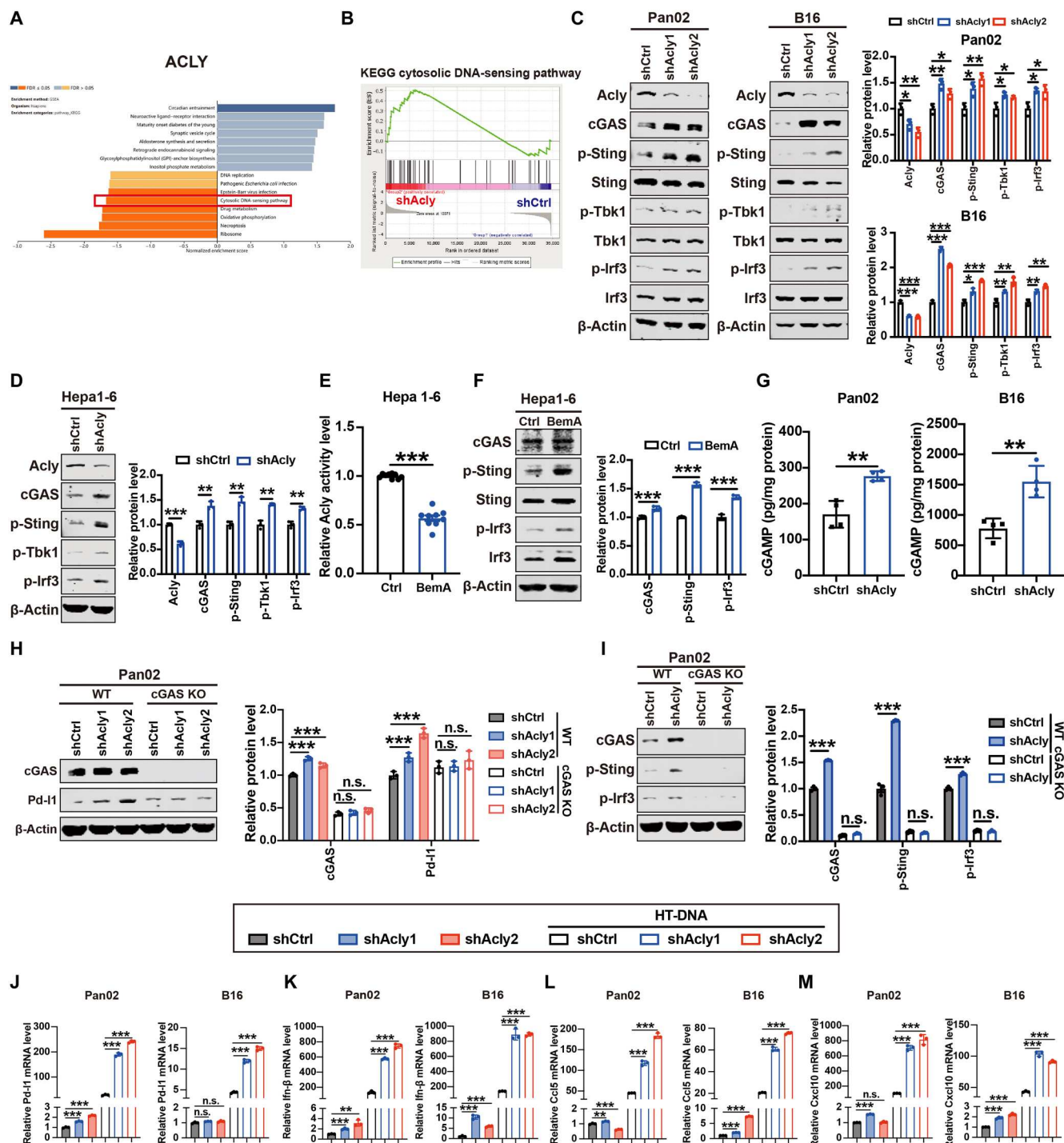**Fig. 2. ACLY inhibition leads to cGAS-STING activation.** (**A**) GSEA (KEGG pathway analysis) of ACLY in pancreatic cancer from TCGA. (**B**) GSEA analysis of RNA sequence data showing a significant enrichment of genes associated with cytoplasmic DNA sensing signaling in shAcly cells versus shCtrl cells. (**C** and **D**) Immunoblot analysis of Acly, cGAS, p-Sting, Sting, p-Tbk1, Tbk1, p-Irf3, and Irf3 expressions in Pan02, B16, and Hepa1-6 cells with Acly knockdown or not. (**E**) Quantification of ACLY activity by ELISA in Hepa1-6 cells with BemA treatment (30 μM) or not. (**F**) Immunoblot analysis of cGAS, p-Sting, and p-Irf3 expression in Hepa1-6 cells with BemA treatment (30 μM) or not. (**G**) Quantification of intracellular cGAMP levels by ELISA in Pan02 cells and B16 cells with Acly knockdown or not. (**H**) Immunoblot analysis of cGAS and Pd-l1 expression in cGAS knockout (KO) or wild-type (WT) Pan02 and B16 cells with Acly knockdown or not. (**I**) Immunoblot analysis of cGAS, p-Sting, and p-Irf3 expression in cGAS KO or WT Pan02 cells with Acly knockdown or not. (**J** to **M**) qPCR analysis of Pd-l1 (J), Ifn-β (K), Ccl5 (L), and Cxcl10 (M) mRNA expressions in Pan02 cells and B16 cells with Acly knockdown or not after HT-DNA stimulation. $n = 3$ biological replicates from one independent experiment (B and J to M); $n = 3$ biological replicates from three independent experiments [(C), (D), (F), (H), and (I)]; $n = 9$ biological replicates from three independent experiments (E) and data are shown as means ± SEM; $n = 4$ biological replicates from two independent experiments (G) and data are shown as means ± SEM. Statistical significance was assessed by one-way ANOVA [(C) and (H) to (M)] and unpaired t test [(D) to (G)]; *$P < 0.05$; **$P < 0.01$; ***$P < 0.001$.

production was observed after ACLY inhibition, further confirming the direct activation of ACLY inhibition on cGAS. Furthermore, ACLY inhibition failed to activate the downstream STING signaling and induce PD-L1 expression when cGAS was knocked out (Fig. 2, H and I), excluding the cGAS-independent activation of the STING pathway by ACLY inhibition. In addition, cGAS-STING pathway downstream targets PD-L1 and Ifn-β, as well as ISGs (Ccl5 and Cxcl10), which are responsible for T cell recruitment, were up-regulated after Acly deficiency, and these target genes were more significantly elevated under double-stranded DNA (dsDNA) stimulation (Fig. 2, J to M). Furthermore, as T cells also express PD-L1 (5, 6), we further tested the role of pharmacologic ACLY inhibition in T cells. Since BemA is a liver-specific ACLY inhibitor, we used another effective and specific ACLY inhibitor (SB204990) (30) to inhibit the ACLY activity of T cells. The inhibition of ACLY activity was confirmed in the human T lymphocyte cell line (Jurkat) after SB204990 treatment (fig. S2A). As shown in fig. S2 (B and C), pharmacologic inhibition of ACLY in T cells failed to activate the cGAS-STING pathway or up-regulate PD-L1, suggesting that ACLY inhibition–induced PD-L1 expression may be cancer cell–specific. Collectively, these findings suggest that ACLY inhibition in cancer cells activates the cGAS-STING pathway to increase PD-L1 and promote T cell recruitment.

ACLY inhibition–induced mitochondrial damage triggers mtDNA leakage to activate cGAS-STING signaling

We next sought to elucidate the mechanism involved in ACLY inhibition–induced cGAS-STING activation. Since the cGAS-STING pathway is known to functionally detect the presence of cytosolic DNA (19, 20), we first tested whether ACLY inhibition causes an increase in cytosolic DNA, thereby triggering activation of the cGAS-STING signaling. In theory, cytosolic DNA could originate from either the nucleus or the mitochondria. To determine the source of cytosolic DNA after Acly deficiency, we purified DNA from cytosolic extracts and found that cytosolic DNA in Acly-deficient cells was mainly mtDNA, as evidenced by increases in Nd1 and Cox1, instead of nuclear DNA, as represented by Tert (fig. S3A). A markedly increased amount of cytosolic dsDNA outside of the mitochondria was observed in Acly-deficient cells in comparison to shCtrl cells (Fig. 3A), supporting ACLY inhibition–induced mtDNA release.

To further investigate whether mtDNA release into the cytosol is responsible for activation of the cGAS-STING signaling in Acly-deficient cells, an established protocol for depleting cellular mtDNA by low-concentration ethidium bromide (EtBr) was used (31). As expected, depletion of cellular mtDNA substantially diminished Acly knockdown–induced increases in cGAS, p-Sting, and p-Irf3 protein levels (Fig. 3B), as well as Ifn-β mRNA levels (Fig. 3C). Furthermore, ACLY inhibition caused mitochondrial damage and dysfunction, as shown by a reduction in oxygen consumption rate (OCR) (Fig. 3D) and a marked increase in mitochondrial reactive oxygen species (ROS) after knockdown of Acly expression (Fig. 3E). As shown in Fig. 3E, more oxidative damages of cytosolic DNA outside of the mitochondria were observed in Acly-deficient cells in comparison to shCtrl cells, suggesting that ACLY inhibition leads to the release of oxidized mtDNA. Of note, mitochondria-targeted antioxidant mitoTEMPO completely blocked the increase in mitochondrial ROS after Acly deficiency (fig. S3B) and substantially diminished Acly inhibition–induced Pd-l1, p-Sting and p-Irf3

protein levels as well as Ifn-β mRNA levels (Fig. 3, G to I). Together, these findings suggest that ACLY inhibition induces mitochondrial damage and dysfunction, resulting in the release of oxidized mtDNA into the cytosol to activate cGAS-STING signaling in cancer cells.

ACLY inhibition causes PUFA peroxidation to induce mitochondrial damage and cGAS-STING activation

We further assessed how ACLY inhibition induced mitochondrial damage. Cancer cells often sustain higher de novo fatty acid synthesis to prevent the uptake of excessive PUFAs, which renders cells more susceptible to apoptosis through lipid peroxidation (32). As ACLY is the key enzyme of de novo fatty acid synthesis, we hypothesized that ACLY inhibition might lead to intercellular PUFA accumulation. Excitingly, liquid chromatography–mass spectrometry (LC-MS) lipidomic analysis showed that Acly deficiency in Pan02 cells increased the levels of omega 3 (n-3) and n-6 PUFAs, including α-linolenic acid (ALA) (18:3), arachidonic acid (ARA) (20:4), and eicosapentaenoic acid (EPA) (20:5) (Fig. 4A). Moreover, increased expression of fatty acid transporter CD36, also known as a fatty acid translocase, which is responsible for fatty acid uptake, was observed after ACLY knockdown in cancer cells (Fig. 4B). In addition, tumor ACLY expression negatively correlated with CD36 expression in human cancer (Fig. 4C and fig. S3C). Therefore, these results suggest that ACLY inhibition facilitates the uptake of excessive PUFAs in cancer cells. Furthermore, we also revealed that excessive PUFA supplementation reduced de novo fatty acid synthesis, as evidenced by decreased ACLY (fig. S3D). Therefore, both the ACLY loss and PUFA supplementation resulted in decreased de novo fatty acid synthesis and increased PUFA uptake.

It is accepted that PUFAs are highly susceptible to lipid peroxidation under oxidative stress (33). As a maker of lipid peroxidation (34), malondialdehyde (MDA) production was significantly elevated after PUFA supplementation (Fig. 4D). Similarly, Acly knockdown markedly enhanced MDA levels in cancer cells (Fig. 4E). In line with ACLY inhibition (Fig. 3E), PUFA (ALA, ARA, or EPA) treatment led to mitochondrial damage, as evidenced by increased mitochondrial ROS (Fig. 4F). Blockade of PUFA uptake by the CD36 inhibitor, sulfosuccinimidyl oleate (SSO) (35), effectively reduced the elevated mitochondrial ROS in Acly-deficient cells (Fig. 4G), indicating that ACLY inhibition–induced mitochondrial damage depends on PUFA accumulation.

We next examined whether ACLY inhibition–induced PUFA peroxidation was responsible for cGAS-STING activation. Consistent with ACLY inhibition, PUFA (ALA, ARA, or EPA) treatment obviously activated the cGAS-STING pathway in cancer cells (Fig. 4H). Moreover, in contrast to ALA, treatment with docosahexaenoic acid (DHA) (22:6) had little effect on the cGAS-STING pathway activation (fig. S3E), suggesting that different types of PUFAs may have distinct effects, at least in pancreatic cancer and melanoma. In addition, although LA (18:2) was not detected in Pan02 cells by LC-MS lipidomic analysis, which could possibly be attributed to its low abundance within the in vitro cell culture system, excessive exogenous LA supplementation was also observed to induce mitochondrial damage and activate the cGAS-STING pathway, as supported by elevated p-Sting and p-Irf3 protein levels as well as Ifn-β mRNA levels (fig. S3, F to H). Furthermore, depletion of mitochondrial ROS abrogated PUFA-induced activation of the cGAS-STING pathway, as evidenced by no difference
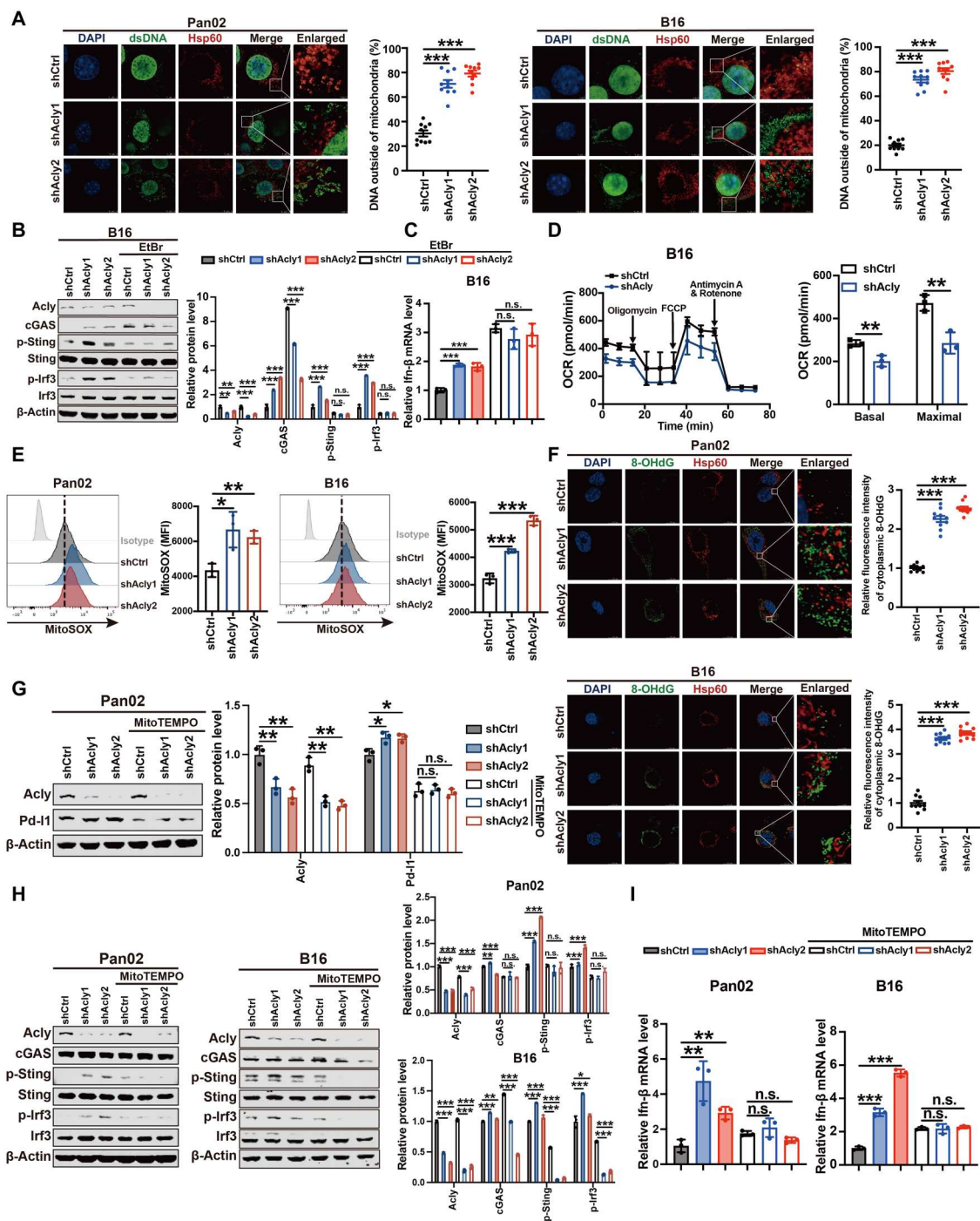
Fig. 3. ACLY inhibition–induced mitochondrial damage triggers mtDNA leakage to activate cGAS-STING signaling. (**A**) Immunofluorescence costaining of anti-dsDNA (green), anti-Hsp60 (red), and 4′,6-diamidino-2-phenylindole (DAPI) (blue) in Pan02 cells and B16 cells with Acly knockdown or not. The percentage of dsDNA (green) outside of mitochondria (red) was quantified. Scale bars, 5 μm. (**B**) Immunoblot analysis of indicated protein expressions in B16 cells with Acly knockdown or not after EtBr treatment. (**C**) qPCR analysis of Ifn-β mRNA expression in B16 cells with Acly knockdown or not after EtBr treatment. (**D**) Seahorse analysis of oxygen consumption rate (OCR) and maximal respiration in B16 cells with Acly knockdown or not. (**E**) Flow staining and MFI of mitoSOX in Pan02 cells and B16 cells with Acly knockdown. (**F**) Immunofluorescence costaining of anti-DNA damage (8-OHdG) (green), anti-Hsp60 (red), and DAPI (blue) in Pan02 cells and B16 cells with Acly knockdown or not. The relative fluorescence intensity of cytoplasmic 8-OHdG (green) outside of mitochondria (red) was quantified. Scale bars, 11.5 μm. (**G**) Immunoblot analysis of indicated protein expressions in Pan02 cells with Acly knockdown or not after mitoTEMPO treatment (10 μM). (**H**) Immunoblot analysis of indicated protein expressions in Pan02 cells and B16 cells with Acly knockdown or not after mitoTEMPO treatment (10 μM). (**I**) qPCR analysis of Ifn-β mRNA expression in Pan02 cells and B16 cells with Acly knockdown or not after mitoTEMPO treatment (10 μM). $n = 10$ biological replicates from two independent experiments [(A) and (F)] and data are shown as means ± SEM; $n = 3$ biological replicates from three independent experiments [(B), (G), and (H)]; $n = 3$ biological replicates from one independent experiment [(C) to (E) and (I)]. Statistical significance was assessed by one-way ANOVA [(A) to (C) and (E) to (I)] and unpaired t test (D); *$P < 0.05$; **$P < 0.01$; ***$P < 0.001$.
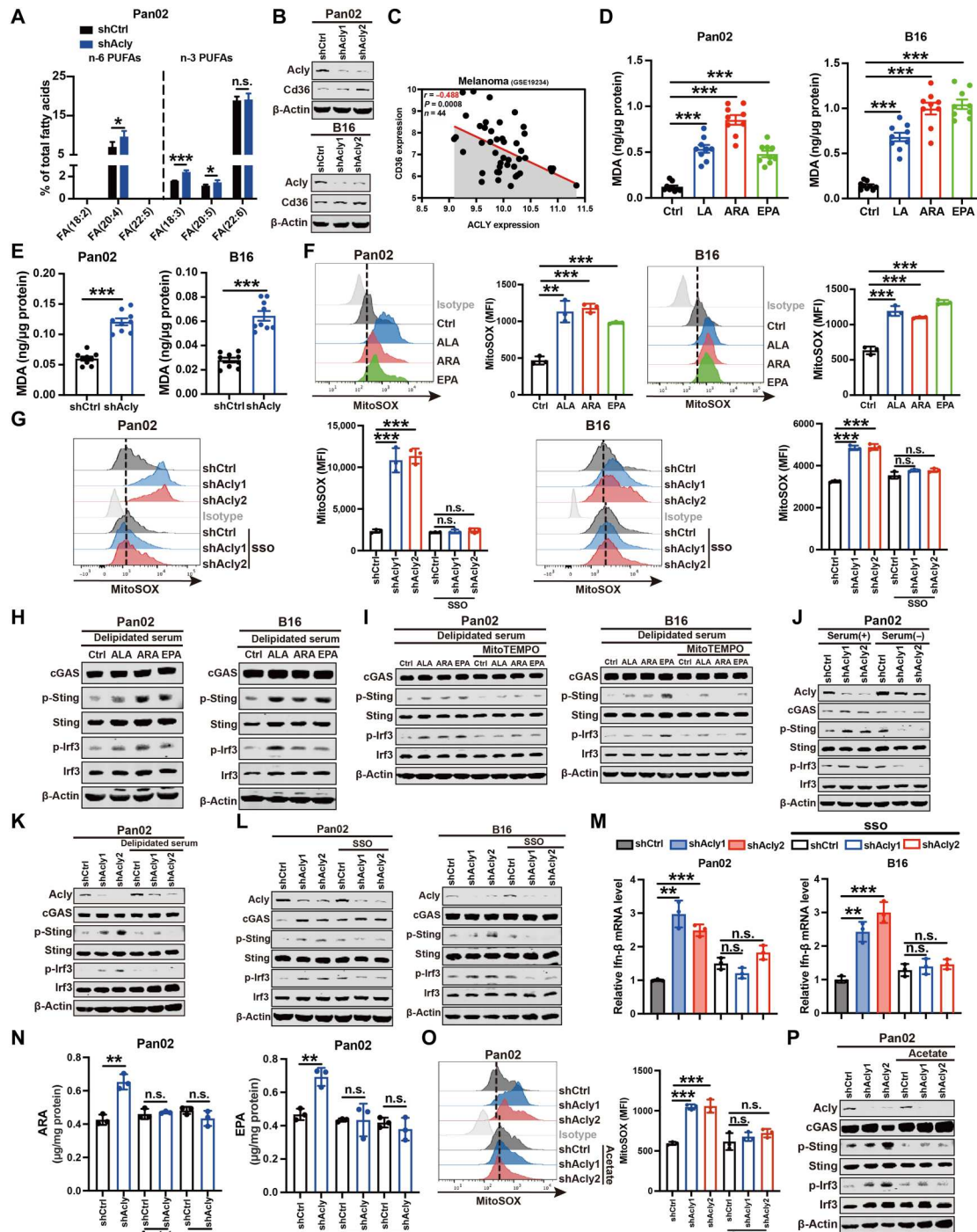
Fig. 4. ACLY inhibition causes PUFA peroxidation to induce mitochondrial damage and cGAS-STING activation. (**A**) LC-MS lipidomic assay of the proportion of n-6 and n-3 PUFAs of total fatty acids in indicated cells. (**B**) Immunoblot analysis of Cd36 expression in indicated cells. (**C**) Pearson's correlation between ACLY and CD36 expression in human melanoma dataset ($n = 44$ patients). (**D** and **E**) Quantification of malondialdehyde (MDA) contents by ELISA in indicated cells after PUFA treatment (50 μM) (D) or Acly deficiency (E). (**F** and **G**) Flow staining and MFI of mitoSOX in indicated cells after PUFA treatment (50 μM) (F) or sulfosuccinimidyl oleate (SSO) treatment (30 μM) (G). (**H** to **L**) Immunoblot analysis of indicated protein expressions in indicated cells after PUFA treatment (50 μM) (H), mitoTEMPO treatment (10 μM) (I), serum deprivation (J), delipidated serum treatment (K), or SSO treatment (30 μM) (L). (**M**) qPCR analysis of Ifn-β mRNA expression in indicated cells after SSO treatment (30 μM). (**N**) Quantification of intracellular ARA and EPA levels by ELISA in indicated cells after acetate treatment (5 mM) or SSO treatment (30 μM). (**O**) Flow staining and MFI of mitoSOX in indicated cells after acetate treatment (5 mM). (**P**) Immunoblot analysis of indicated protein expressions in indicated cells after acetate treatment (5 mM). $n = 5$ (A) and $n = 3$ [(F), (G), and (M) to (O)] biological replicates from one independent experiment; $n = 3$ biological replicates from three independent experiments [(B), (H) to (L), and (P)]; $n = 9$ biological replicates from three independent experiments [(D) and (E)] and data are shown as means ± SEM. The quantification [(B), (H) to (L), and (P)] was shown in fig. S3. Statistical significance was assessed by one-way ANOVA [(B), (D), and (F) to (P)] and unpaired t test [(A) and (E)]; *$P < 0.05$; **$P < 0.01$; ***$P < 0.001$.

of p-Sting and p-Irf3 protein levels as well as Ifn-β mRNA levels in PUFA-stimulated cells after mitoTEMPO exposure (Fig. 4I), together implying that excessive PUFAs are sufficient to activate the cGAS-STING pathway via lipid peroxidation–induced mitochondrial damage.

We further assessed whether ACLY inhibition–induced cGAS-STING pathway activation relies on PUFA uptake. For cells in culture, PUFAs come from serum added to supplement medium, and thus we remove PUFAs from the cellular environment via serum deprivation or delipidated serum. As shown in Fig. 4 (J and K), serum deprivation or delipidated serum blocked ACLY knockdown–induced activation of the cGAS-STING pathway in Pan02 cells. Moreover, adding back only palmitic (16:0) and oleic (18:1) acids to delipidated serum failed to activate cGAS-STING signaling in shACLY cells (fig. S3I). The increased phosphorylation of Sting and Irf3 proteins as well as Ifn-β mRNA expression in Acly-deficient cells was abolished after suppression of PUFA uptake by CD36 inhibitor SSO (Fig. 4, L and M), suggesting that ACLY inhibition activates the cGAS-STING pathway through PUFA accumulation. In addition, acetate metabolism has been shown to compensate for acetyl–CoA and de novo fatty acid synthesis in the absence of ACLY (11, 16). After confirming that de novo fatty acid synthesis is suppressed in shACLY cells, as supported by a substantial reduction in acetyl–CoA levels (fig. S3J), we further demonstrated that acetate supplementation effectively reduced the elevated intracellular PUFA (ARA and EPA) levels and mitochondrial ROS and blocked the activation of cGAS-STING signaling in Acly-deficient cells (Fig. 4, N to P). Collectively, these findings imply that suppression of ACLY enzyme-mediated acetyl–CoA and de novo fatty acid synthesis is responsible for PUFA uptake, mitochondrial damage, and cGAS-STING activation.

Low ACLY expression correlates with cGAS-STING activation and exhausted T cell infiltration in human cancers

Next, we verified the correlation between tumor ACLY expression and cGAS-STING activation in tissues of patients with cancer. Immunohistochemical (IHC) staining exhibited a negative correlation between ACLY and cGAS protein expressions in human HCC clinical samples (Fig. 5, A and B). It is known that activation of the cGAS-STING pathway up-regulates PD-L1 in tumor cells (21). Similar to cGAS, we found that tumor ACLY expression also inversely correlated with PD-L1 expression (Fig. 5, A and C). Furthermore, tumor ACLY expression levels showed a significant negative correlation with ISGs, which are target genes of the cGAS-STING pathway, in multiple tumors including HCC, PDAC, and melanoma (Fig. 5, D to F). Together, these results indicate that low ACLY expression correlates with cGAS-STING activation in human cancers.

Consistent with the results showing more intratumoral CD8^{+} T cell infiltration after ACLY inhibition in mouse tumor model (Fig. 1E), it was observed that ACLY expression inversely correlated with CD8^{+} T cell infiltration in human HCC tissues (Fig. 5, G and H). In addition, a negative correlation between tumor ACLY expression and CD8A expression was found in HCC and PDAC datasets (Fig. 5, I and J). Nevertheless, lower tumor ACLY expression was linked to higher expressions of T cell exhaustion markers lymphocyte activation gene-3 (LAG3) and T cell immunoreceptor with Ig and ITIM domains (TIGIT) (Fig. 5, K and L), implying more exhausted T cell infiltration in low ACLY-expressed tumors. In agreement with the suppressive effect of ACLY inhibition on tumor growth in immunodeficient mice but not in immunocompetent mice (Fig. 1A and fig. S1B), low tumor ACLY expression predicted better clinical outcome in cancer patients with CD8^{+} T cell–deficient tumors, while in tumors with enriched CD8^{+} T cell infiltration, patients with low tumor ACLY expression had significantly poorer survival (Fig. 5M and fig. S4A), supporting the immunosuppressive role of low ACLY in multiple types of cancers. Collectively, these data suggest that low ACLY expression correlates with cGAS-STING activation and exhausted T cell infiltration in human cancers.

ACLY inhibition overcomes cancer resistance to anti–PD-L1 therapy depending on cGAS

cGAS-STING is essential for the antitumor effect of immune checkpoint blockade (36). Building on our above observations that ACLY inhibition leads to cGAS-STING activation, we sought to determine whether ACLY inhibition enhanced the therapeutic efficacy of αPD-L1 antibody in vivo using primary αPD-(L)1 therapy tolerance tumor model (Pan02 pancreatic cancer and B16 melanoma models). Administration of αPD-L1 as a monotherapy had limited effect on tumor growth but caused significantly greater tumor suppression after Acly deficiency in Pan02 pancreatic cancer (Fig. 6, A and B, and fig. S5, A and B) and B16 melanoma models (fig. S5, C and D). We further used a secondary αPD-(L)1 therapy tolerance tumor model (Hepa1-6 liver cancer with CD38 overexpression, which is a major mechanism of tumor resistance to immune checkpoint therapy) (37). Similarly, ACLY inhibitor BemA markedly enhanced the antitumor effects of αPD-L1 blockade in the Hepa1-6–CD38 liver cancer model (Fig. 6, C and D). Further analysis of immune infiltration by flow cytometry showed that αPD-L1 antibody treatment promoted CD8^{+} T cell infiltration and the function of CD8^{+} T cells to secrete IFN-γ and GZMB whereas reduced the proportion of exhausted PD-1^{+}CD8^{+} T cells in tumors with ACLY knockdown (Fig. 6, E to H). Together, these results indicate that combined ACLY inhibition plus immune checkpoint blockade significantly increase cytotoxic T cell infiltration and enhance the antitumor effects in αPD-(L)1 therapy–resistant tumors.

To further confirm T cell populations accounting for the combinational antitumor effect of ACLY inhibition and αPD-L1 antibody, we depleted CD8^{+} T cells in mice inoculated subcutaneously with shAcly cells. Notably, the significantly repressed tumor burden after αPD-L1 treatment in ACLY-deficient tumors was reversed after treatment with depleting antibody against CD8 (Fig. 6, I and J), and the depletion of CD8^{+} T cells in tumors of mice was confirmed by flow cytometry (Fig. 6K). Furthermore, when BemA combined with αPD-L1 treatment resulted in complete tumor regression in comparison to αPD-L1 treatment alone in αPD-(L)1 therapy–resistant liver cancer model (Hepa1-6–CD38), these mice without tumors were rechallenged with Hepa1-6–CD38 cells. Excitingly, these mice did not develop obvious tumors compared with age-matched wild-type mice (Fig. 6L), suggesting that ACLY inhibition combined with αPD-L1 therapy leads to durable antitumor immunity. In addition, BemA treatment did not exert any additional synergic effects with αPD-L1 treatment in mice bearing ACLY-deficient tumors (Fig. 6, M and N), demonstrating that the combinational antitumor effect of pharmacological ACLY inhibition with αPD-L1 therapy is mainly due to ACLY inhibition in the cancer cells versus the stroma. Also, these results indicate that the combined
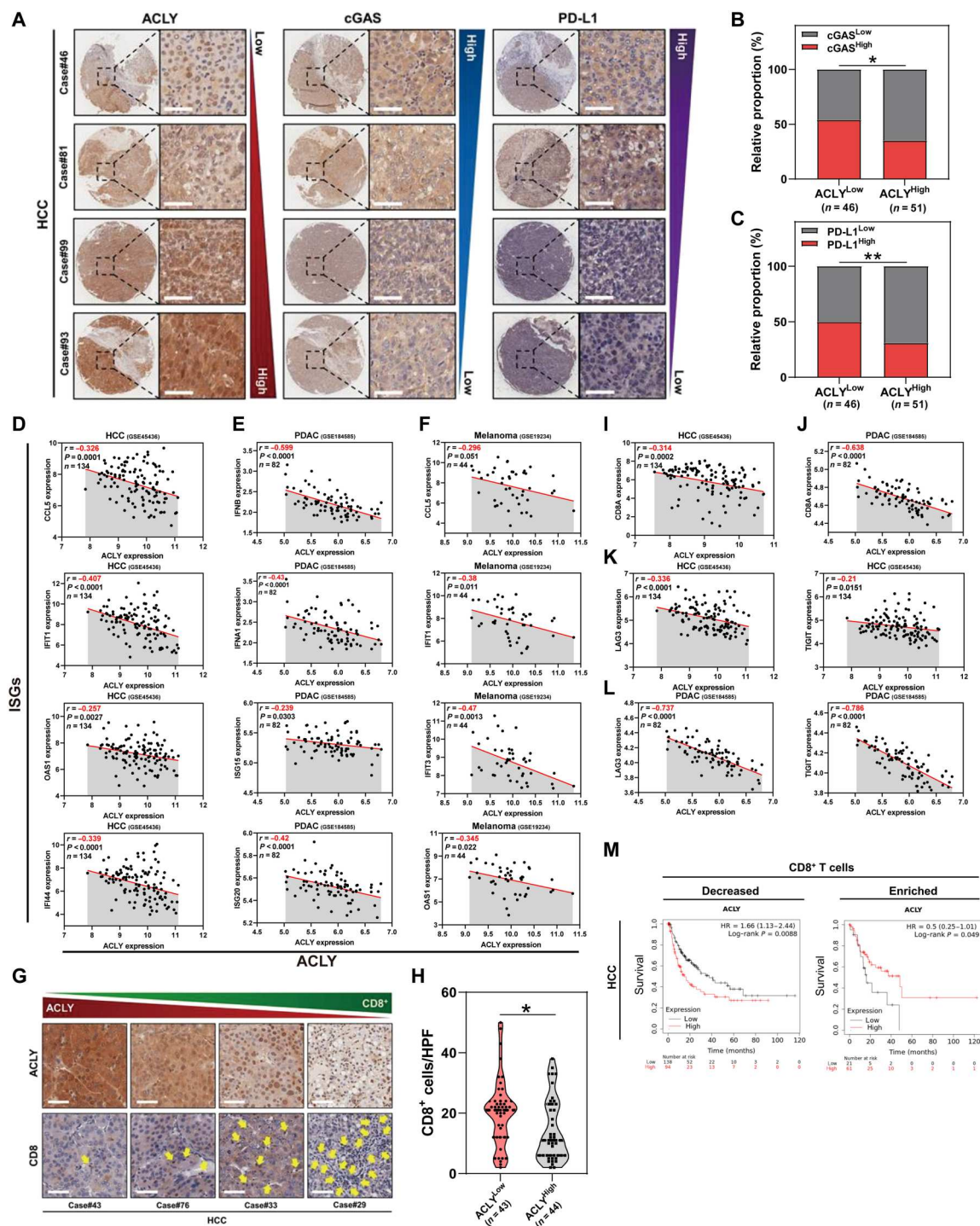
Fig. 5. Low ACLY expression correlates with cGAS-STING activation and exhausted T cell infiltration in human cancers. (**A** to **C**) Immunohistochemical staining of ACLY, cGAS, and PD-L1 expression in patients with HCC (A). Scale bars, 50 μm. On the basis of the intensity of staining (protein expression), the patients were subdivided into two groups: low (staining scores 0 to 1) and high (staining scores 2 to 3) expression groups. Correlation analysis of ACLY expression with cGAS or PD-L1 expression in HCC tissues (B and C) ($n = 97$ patients). (**D** to **F**) Pearson's correlation between ACLY expression and ISGs in HCC (D), PDAC (E), and melanoma (F) datasets ($n = 134$ patients with HCC, $n = 82$ patients with PDAC, $n = 44$ patients with melanoma). (**G** and **H**) Immunohistochemistry of clinical HCC samples reveals an inverse correlation between tumor ACLY expression (top) and CD8^{+} T cell infiltration (bottom). The yellow arrows represent CD8^{+} T cell infiltration (G). Scale bars, 50 μm. Correlation analysis of ACLY expression with CD8^{+} T cell number per HPF ($n = 87$ patients). The dashed line across the violin plots represents the quartiles and the full line depicts the median (H). (**I** and **J**) Pearson's correlation between ACLY and CD8A expression in HCC (I) and PDAC (J) datasets. (**K** and **L**) Pearson's correlation between ACLY expression and markers of T cell exhaustion (LAG3 and TIGIT) in HCC (K) and PDAC (L) datasets. (**M**) Kaplan-Meier analysis of survival in HCC according to the expression of ACLY in the group with decreased or enriched intratumoral CD8^{+} T cell infiltration. Statistical significance was assessed by Chi-square test [(B) and (C)] and unpaired t test (H); *$P < 0.05$; **$P < 0.01$.
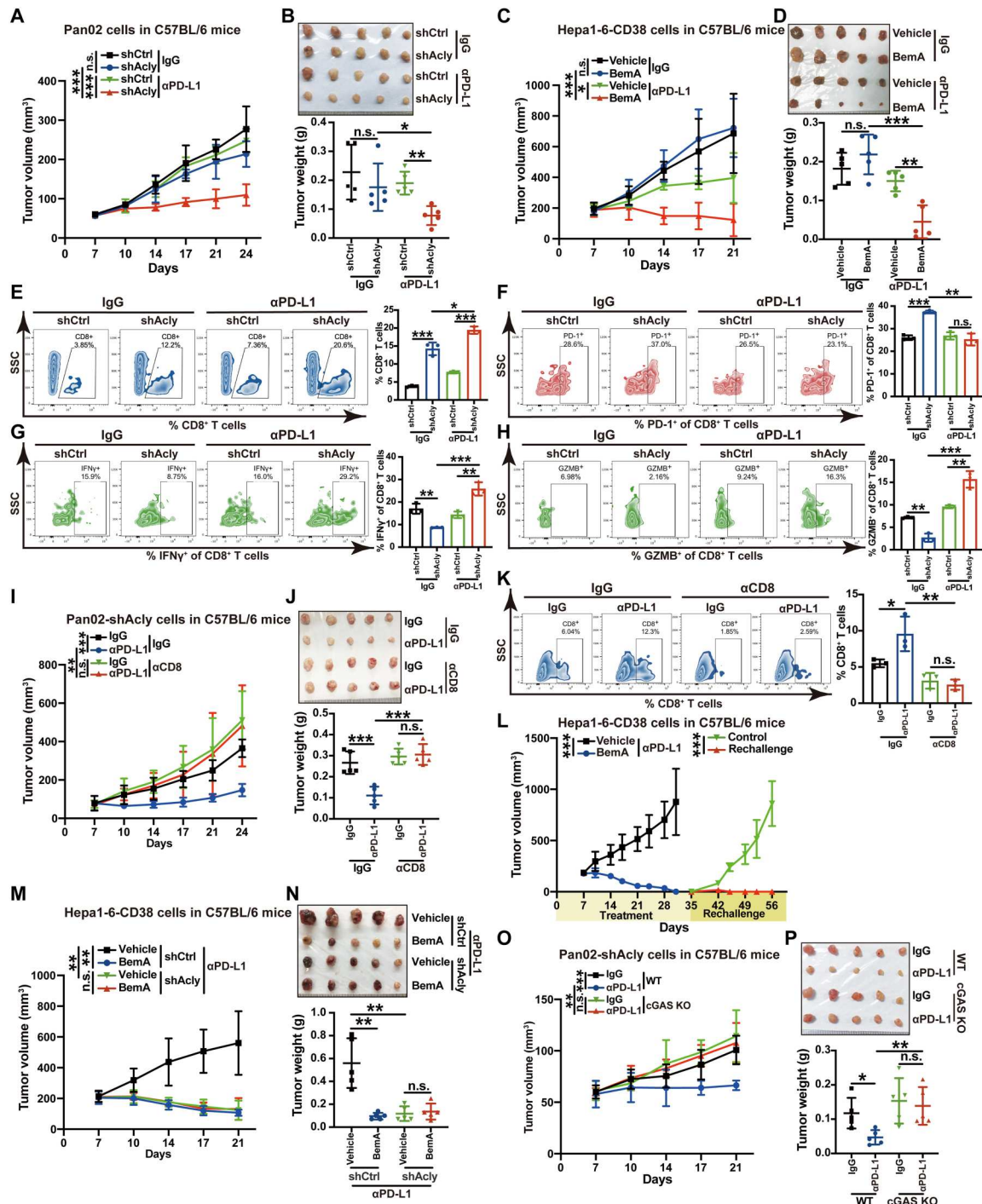
Fig. 6. ACLY inhibition overcomes cancer resistance to anti–PD-L1 therapy depending on cGAS. (**A** and **B**) Tumor growth (A) and tumor burdens (B) in C57BL/6 mice injected subcutaneously with shAcly or shCtrl Pan02 cells with αPD-L1 antibodies treatment. One additional independent experiment was performed that yielded similar results (fig. S5, A and B). (**C** and **D**) Tumor growth (C) and tumor burdens (D) in C57BL/6 mice injected subcutaneously with Hepa1-6–CD38 cells with treatment of BemA and αPD-L1 antibodies either alone or in combination. (**E** to **H**) Flow staining and frequency of indicated cells in tumors of indicated groups. (**I** and **J**) Tumor growth (I) and tumor burdens (J) in C57BL/6 mice injected subcutaneously with Pan02 cells with Acly deficiency with the treatment of αPD-L1 antibodies after CD8 depletion. (**K**) Flow staining and frequency of CD8^{+} T cells in tumors of indicated groups. (**L**) Tumor growth in C57BL/6 mice reinjected subcutaneously with Hepa1-6–CD38 cells after complete tumor regression by BemA combined with αPD-L1 treatment ($n = 6$ mice for combined treatment and $n = 5$ mice for tumor rechallenge). (**M** and **N**) Tumor growth (M) and tumor burdens (N) in C57BL/6 mice injected subcutaneously with shAcly or shCtrl Hepa1-6–CD38 cells with treatment of BemA and αPD-L1 antibodies either alone or in combination. (**O** and **P**) Tumor growth (O) and tumor burdens (P) in C57BL/6 mice injected subcutaneously with shAcly Pan02 cells with cGAS KO or not after the treatment of αPD-L1 antibodies. $n = 5$ mice per group from one independent experiment [(A) to (D), (I), (J), and (M) to (P)]; $n = 3$ biological replicates from one independent experiment [(E) to (H) and (K)]. Statistical significance was assessed by two-way ANOVA [(A), (C), (I), (L), (M), and (O)] and one-way ANOVA [(B), (D) to (H), (J), (K), (N), and (P)]; *$P < 0.05$; **$P < 0.01$; ***$P < 0.001$.

effect of BemA and αPD-L1 treatment relies on ACLY inhibition by BemA rather than AMP-activated protein kinase (AMPK) activation, which is another known target for BemA (38). cGAS knockout (KO) completely abrogated the enhanced therapeutic efficacy of αPD-L1 antibody in tumors with Acly deficiency (Fig. 6, O and P). Therefore, these findings suggest that pharmacological and genetic inhibition of ACLY in cancer cells overcomes cancer resistance to αPD-L1 therapy in a cGAS-dependent manner.

Dietary PUFA supplementation mirrors the enhanced efficacy of PD-L1 blockade by ACLY inhibition

Recently, dietary PUFAs have attracted great attention for their potential anticancer effects (39). On the basis of our above findings that ACLY inhibition activates cGAS-STING through PUFA oxidation and direct addition of PUFAs effectively causes the activation of the cGAS-STING pathway in cancer cells, we therefore evaluated whether PUFA supplementation could sensitize cancers to immunotherapy, similarly to ACLY inhibition. Excitingly, oral gavage of PUFAs (ALA, EPA, or LA) combined with PD-L1 blockade marked tumor regression in the mouse model of Pan02 pancreatic cancer (Fig. 7, A to D, and fig. S6, A and B), implying that dietary PUFA supplementation can reverse the resistance of cancers to immunotherapy. Furthermore, flow cytometry analysis of immune infiltration revealed that PUFAs (ALA, EPA, or LA) and PD-L1 antibody combination significantly increased $CD8^+$ T cell infiltration whereas decreased the proportion of exhausted PD-1^+CD8^+ T cells in tumors (Fig. 7, E to H, and fig. S6, C and D). cGAS KO completely abrogated the synergic therapeutic efficacy of dietary PUFA supplementation (ALA or EPA) with αPD-L1 treatment (Fig. 7, I to L), suggesting that dietary PUFA supplementation enhances the efficacy of PD-L1 blockade depending on cGAS. Together, our data indicate that dietary PUFA supplementation is sufficient to mimic the enhanced efficacy of αPD-L1 therapy by ACLY inhibition in a cGAS-dependent manner.

DISCUSSION

Aberrant lipid metabolism is one of the most important metabolic alterations in cancer (11, 12). Lipid synthesis is commonly enhanced to meet the increased demand for rapid cancer cell growth and tumor formation (11, 12). Mounting pieces of evidence support the crucial role of lipid synthesis in tumor immunity, but major studies have focused on immune cells themselves so far (40). For instance, it has been demonstrated that lipid accumulation in dendritic cells impairs their ability to stimulate allogeneic T cells or present tumor-associated antigens (41). Moreover, lipid droplet–dependent fatty acid metabolism polarizes myeloid cells into immunosuppressive tumor-associated macrophages (42). However, how and whether fatty acid synthesis of cancer cells regulates tumor immune evasion or antitumor immunity is largely unclear. Here, we unexpectedly discover that inhibition of ACLY, the upstream rate-limiting enzyme of de novo fatty acid synthesis, up-regulates the PD-L1 immune checkpoint and induces T cell dysfunction to drive immunosuppression, despite that ACLY inhibition impairs cancer cell growth in culture and in immunodeficient mice, consistent with many previous reports (14, 15).

Note that de novo fatty acid synthesis and exogenous fatty acid uptake are important compensatory mechanisms for cancer cells to sustain their lipid demands under conditions of metabolic stress

(11, 12). Cancer cells frequently maintain higher de novo fatty acid synthesis to prevent the uptake of excessive PUFAs, which are highly susceptible to peroxidation and render cancer cells more sensitive to oxidative stress–induced cell death (32, 33). In this study, ACLY inhibition impairs de novo fatty acid synthesis and therefore triggers an increase in demand for uptaking more PUFAs. Subsequently, PUFA accumulation leads to lipid peroxidation and mitochondrial damage, which further increases the cytoplasmic release of mtDNA to up-regulate PD-L1 via activation of cGAS-STING signaling (Fig. 7M). Therefore, since ACLY inhibition may carry an immunosuppressive effect, ACLY inhibitor monotherapy for cancers in preclinical models and clinical trials needs careful consideration and evaluation. In addition to ACLY, fatty acid synthesis is controlled by a series of metabolic enzymes in the cytoplasm, especially two other rate-limiting enzymes acetyl-CoA carboxylase and fatty acid synthase (11). Thus, the role of other key lipogenic enzymes in tumor immunity needs to be further investigated.

Dietary restriction of calories or special amino acids has currently drawn great interest in cancer treatment (39). However, these approaches also bring obvious adverse events to patients with cancer, including weight loss, fatigue, and weakness (39). Currently, strategies of supplementing specific nutrients rather than restricting diets have emerged as a promising option for cancer therapy. In particular, PUFAs represent a class of lipids that can exert a potential antitumor effect. Some prospective analyses of >1000 patients with colorectal cancer showed that a high intake of marine n-3 PUFAs had lower cancer-associated deaths and longer disease-free survival (43, 44). Furthermore, it has recently been reported that dietary PUFAs induce ferroptosis in cancer cells via lipid peroxidation (45, 46). Although PUFA supplementation has shown a direct antitumor effect, the role of PUFAs in tumor immunity is controversial as PUFAs have been shown to not only promote stromal cell–mediated immunosuppression (47, 48) but also potentiate $CD8^+$ T cell–mediated antitumor immunity (49, 50). In addition, whether and how PUFA supplementation affects tumor cell metabolism to further regulate antitumor immune responses is largely unknown. In this work, to confirm that ACLY inhibition–induced PUFA accumulation is responsible for the activation of cGAS-STING signaling, we also demonstrate that PUFA supplementation is sufficient to activate cGAS-STING signaling via lipid peroxidation in cancer cells, indicating the potential immunosuppressive role of PUFAs. Dietary PUFA supplementation markedly enhances the efficacy of PD-L1 blockade in immunotherapy-resistant tumors, mimicking the effect of ACLY inhibition. Collectively, our findings also uncover the potential role of PUFAs in cancer immunity and imply that dietary PUFA supplementation combined with immune checkpoint blockade may represent a particularly attractive strategy for cancer treatment and is worthy of further investigation.

Recently, increasing pieces of evidence show that the cGAS-STING pathway plays a dichotomous role in the regulation of tumor immunity, either activating or suppressing antitumor immune responses (21, 24). Although cGAS-STING pathway activation is known to promote T cell priming and intratumoral T cell infiltration by the production of IFNs, activation of this signaling pathway has been shown to up-regulate PD-L1 on the surface of tumor cells and thus attenuate the activity of cytotoxic T cells, as demonstrated in multiple types of cancers (25, 51, 52). In this study, we find that ACLY inhibition–mediated cGAS-STING
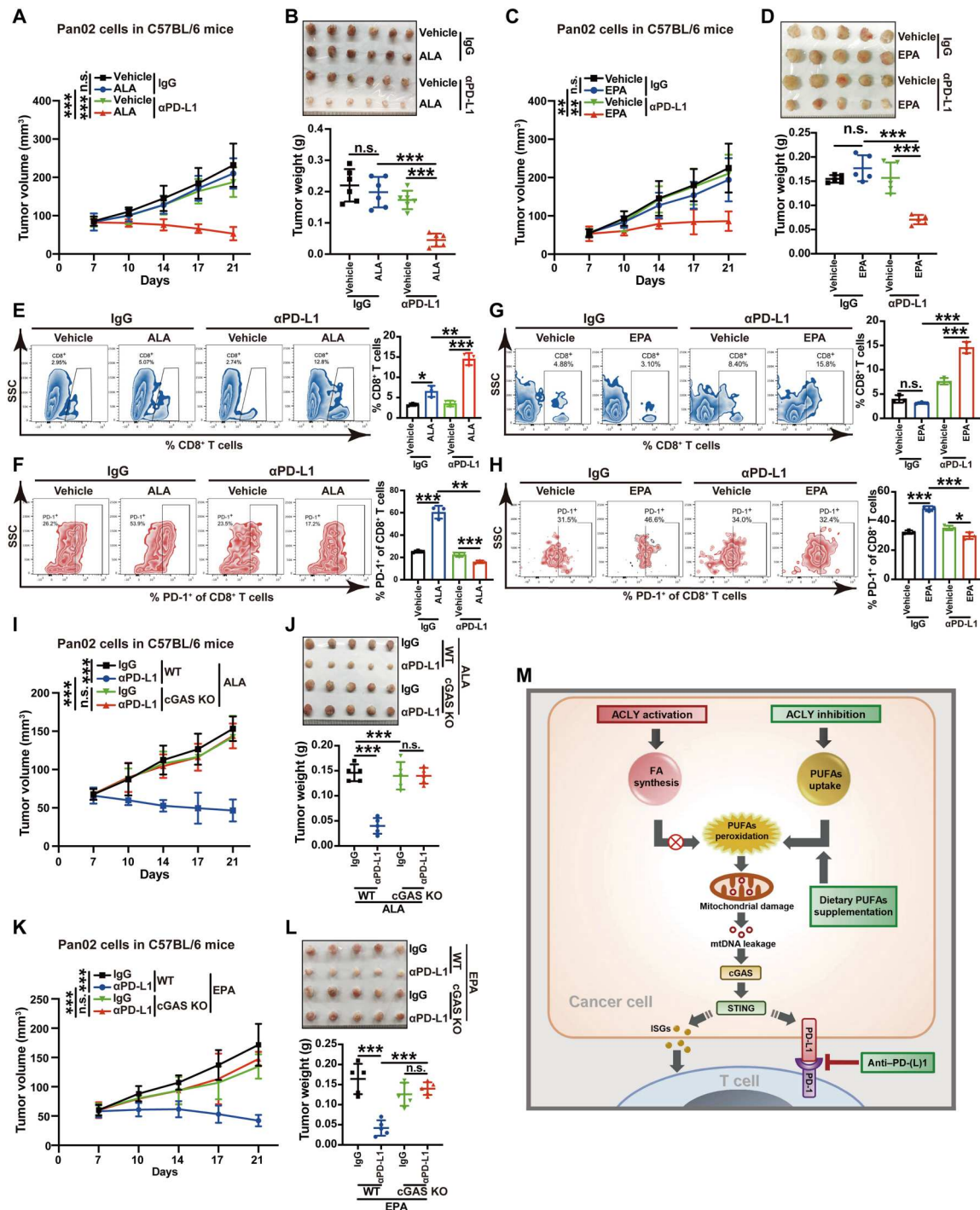
Fig. 7. Dietary PUFA supplementation mirrors the enhanced efficacy of PD-L1 blockade by ACLY inhibition. (**A** and **B**) Tumor growth (A) and tumor burdens (B) in C57BL/6 mice injected subcutaneously with Pan02 cells with the treatment of ALA and αPD-L1 antibodies either alone or in combination. (**C** and **D**) Tumor growth (C) and tumor burdens (D) in C57BL/6 mice injected subcutaneously with Pan02 cells with treatment of EPA and αPD-L1 antibodies either alone or in combination. (**E** and **F**) Flow staining and frequency of indicated cells in indicated tumors. (**G** and **H**) Flow staining and frequency of indicated cells in indicated tumors. (**I** and **J**) Tumor growth (I) and tumor burdens (J) in C57BL/6 mice injected subcutaneously with Pan02 cells with cGAS KO or not with the treatment of ALA and αPD-L1 antibodies either alone or in combination. (**K** and **L**) Tumor growth (K) and tumor burdens (L) in C57BL/6 mice injected subcutaneously with Pan02 cells with cGAS KO or not with treatment of EPA and αPD-L1 antibodies either alone or in combination. (**M**) Summary scheme. ACLY activation sustains higher de novo fatty acid (FA) synthesis to prevent excessive PUFA uptake, while ACLY inhibition reduces de novo FA synthesis but enhances the uptake of excessive PUFAs, which induces mitochondrial damage via lipid peroxidation, further triggering mtDNA leakage to activate the cGAS-STING pathway and lastly boosting PD-(L)1 blockade efficacy. $n = 6$ mice per group from one independent experiment [(A) and (B)]; $n = 5$ mice per group from one independent experiment [(C), (D), and (I) to (L)]; $n = 3$ biological replicates from one independent experiment [(F), (G), and (M) to (O)]. Statistical significance was assessed by two-way ANOVA [(A), (C), (I), and (K)] and one-way ANOVA [(B), (D) to (H), (J), and (L)]; *$P < 0.05$; **$P < 0.01$; ***$P < 0.001$.

activation increases the expression of PD-L1 in cancer cells and induces T cell dysfunction to drive immunosuppression, compromising the antitumor effect of ACLY inhibition in immunocompetent mice. Thus, although cGAS-STING agonists hold promise as potential anticancer agents, monotherapy of cGAS-STING agonists may bring the side effect of immunosuppression. In clinical trials, STING agonist treatment has encountered profound cancer resistance (22, 23). Fortunately, since tumor PD-L1 expression level is a well-established biomarker of response to immune checkpoint inhibitors (26), combined cGAS-STING agonists with immune checkpoint blockade can mechanistically synergize to suppress tumor growth, as demonstrated in clinical and preclinical models (27, 28). In this study, our findings provide a promising approach to activating the cGAS-STING pathway via targeting lipid metabolism by inhibition of ACLY, the key enzyme of lipid synthesis, for overcoming cancer resistance to αPD-L1 therapy. The combinatorial strategy of ACLY inhibition and αPD-L1 therapy is worth investigating in future clinical trials, especially the known ACLY inhibitor, BemA, which is an FDA-approved low-density lipoprotein cholesterol-lowering agent (18). In addition to ACLY inhibition, whether BemA mediates antitumor immune response and immunotherapy efficacy through other known effects including AMPK activation also needs further study (38).

The importance of the STING pathway as a pharmacologic target has boosted the development of several synthetic STING agonists, according to the structure of natural STING ligands (21). However, the therapeutic efficacy of these agonists is limited because of the poor membrane permeability and low bioavailability (22, 23). An alternative strategy to activate STING signaling is prompting endogenous cGAMP production via cGAS activation. Recently, it has been reported that genotoxic therapies such as chemotherapy and radiotherapy trigger STING pathway activation through cytoplasmic DNA−induced activation of cGAS (53). For example, chemotherapy reagents including cisplatin and paclitaxel activate cancer cell−intrinsic STING signaling via the accumulation of DNA damage (54, 55). However, chemotherapy and radiotherapy frequently cause tumor resistance mainly due to cancer stem cells (CSCs), a subpopulation of cancer cells, responsible for cancer progression, recurrence, and metastasis (56). We have previously demonstrated that ACLY maintains liver CSCs (57), further confirmed by other recent studies (58), and inhibition of ACLY suppresses stemness properties of liver cancer (57). Thus, ACLY inhibition may provide a potential advantage of eradicating CSCs over other therapeutic strategies to activate cGAS-STING, making the combination therapy with ACLY inhibition and immune checkpoint blockade a promising anticancer approach with improved and sustained efficacy.

MATERIALS AND METHODS
Human cancer specimens
Tissue microarrays composed of tumor samples were obtained from patients with pathologically confirmed HCC at Eastern Hepatobiliary Surgery Hospital (Shanghai, China). All procedures were conducted with the approval of the Ethical Committee of the Second Military Medical University and performed in accordance with relevant regulations and guidelines. Patient consent was obtained before the start of the study.

Cell culture
The murine liver cancer cell line Hepa1-6 and melanoma cell line B16 were purchased from the Cell Bank of Type Culture Collection of the Chinese Academy of Sciences (Shanghai Institute of Cell Biology). The murine pancreatic cancer cell line Pan02 was purchased from Cell Resource Center, IBMS, CAMS/PUMC (Beijing, China). All cells were grown in Dulbecco's modified Eagle's medium (Gibco) supplemented with 10% fetal bovine serum (FBS) (Gibco) and cultured in a humidified incubator containing 5% CO_2 at 37°C. Cell lines were authenticated by short tandem repeat (STR) profiling and confirmed to be mycoplasma negative.

Antibodies and reagents
Anti-ACLY (4332), anti-cGAS (31659), anti–p-STING (4332), anti–STING (13647), anti–p-TBK1 (5483), anti–p-IRF3 (29047), and anti-IRF3 (4302) were purchased from Cell Signaling Technology. αPD-L1 (28076-1-AP) and anti-TBK1 (28397-1-AP) were purchased from Proteintech. Anti-ACLY (ab40793), αPD-L1 (ab213480), anti-HSP60 (ab46798), anti-dsDNA (ab27156), anti–DNA damage (8-OHdG) (ab62623), anti-Ki67 (ab16667), and anti-CD8 (ab93278) were purchased from Abcam. Anti-cGAS (sc-515802) was purchased from Santa Cruz Biotechnology. Anti-CD36 (GTX100642) was purchased from GeneTex. Phycoerythrin (PE) anti-mouse CD274 (PD-L1) (124308), fluorescein isothiocyanate anti-mouse CD45 (124308), Brilliant Violet 421 anti-mouse CD279 (PD-1) (135217), Alexa Fluor 647 anti-mouse GZMB (372220), PE anti-mouse IFN-γ (505808), PE/Cyanine7 anti-mouse CD3 (100220), and Brilliant Violet 605 anti-mouse CD8a (100743) were purchased from BioLegend. InVivoMab anti-mouse PD-L1 (B7-H1) (BE0101), anti-mouse CD8a (BE0004), and immunoglobulin G (IgG) isotype (BE0089/BE0090) were purchased from BioXcell.

BemA (HY-12357), SB204990 (HY-16450), linolenic acid (LA) (HY-N7140), ARA (HY-109590), EPA (HY-B0660), ALA (HY-N0728), DHA (HY-B2167), palmitic acid (HY-N0830), oleic acid (HY-N1446), and SSO (HY-112847) were purchased from MCE. MitoTEMPO (16621) was purchased from Cayman. HT-DNA (D6898), EtBr (E7637), sodium acetate (S5636), collagenase IV (C5138), and deoxyribonuclease I (DNase I) (D5025) were purchased from Sigma-Aldrich. MitoSOX Red mitochondrial superoxide indicator (M36008) was purchased from Invitrogen. Lipid-depleted FBS (C3840) was purchased from Vivacell.

Animal models
Male mice at 5 to 6 weeks of age used in the experiments were obtained from the GemPharmatech Co., Ltd (Jiangsu, China). All mice were housed in specific pathogen-free facilities under a 12-hour light/dark cycle and controlled temperature (20° to 25°C) with standard rodent chow (Product Standard No. Q031/0120000099C001-2015, Shanghai Shilin Biologic Science & Technology, China) and water provided ad libitum. To establish subcutaneous tumor models, 1×10^6 Hepa1-6 cells, 2×10^6 Pan02 cells, or 5×10^5 B16 cells were injected subcutaneously into the left thighs of C57BL/6 mice. A total of 5×10^5 Hepa1-6 cells were injected subcutaneously into the left thighs of nude mice. Tumor growth was monitored by measuring the tumor size (length × width^2 × 0.5) twice per week after injection. At 3 to 4 weeks after tumor establishment, all the mice were euthanized to harvest subcutaneous tumors for weight measurement and further tissue analyses. All animal protocols

used in this study were approved by The University Committee on Use and Care of Animals of Second Military Medical University.

In vivo treatments and depletion of CD8^{+} T cells

Before treatment initiation, mice were randomly assigned to indicated groups with similar average tumor volumes. For ACLY inhibitor BemA treatment, mice were intraperitoneally injected with BemA (30 mg/kg body weight) or solvent twice a week for 2 weeks beginning on day 7 after the establishment of Hepa1-6 liver cancer models. For αPD-L1 antibodies treatment, mice were intraperitoneally injected with αPD-L1 antibodies (100 μg per mouse) or IgG isotype control twice a week for 2 weeks beginning on day 7 after the establishment of indicated cancer models. For LA and EPA treatments, mice were administrated with ALA (100 mg/kg body weight), LA (100 mg/kg body weight), EPA (100 mg/kg body weight), or solvent daily by oral gavage for 2 weeks beginning on day 7 after the establishment of Pan02 pancreatic cancer models. For depletion of CD8^{+} T cells in vivo, mice were intraperitoneally injected with anti-CD8a antibodies (100 μg per mouse) or IgG isotype control 3 days and 1 day before tumor implantation and twice weekly thereafter to ensure sustained depletion of CD8^{+} T cells during the experimental period.

shRNA, CRISPR-Cas9, and overexpression

The lentivirus-mediated shRNA expressing vector targeting murine Acly (target sequence #1: 5′-GCTGAATACCGAGGACATT-3′; target sequence #2: 5′-GCTTCATCTCTGGTCTATT-3′) and the lentivirus-mediated CRISPR-Cas9 KO vector targeting murine cGAS (target sequence: 5′-CGGCGGGCAGCTCCGGATCC-3′) were purchased from OBiO Technology (Shanghai, China). The lentiviral plasmids expressing murine CD38 were purchased from GeneChem (Shanghai, China). Cells at 30 to 40% confluency were incubated in a medium containing optimal dilutions of lentivirus mixed with polybrene. Then, cells were subjected to puromycin selection to obtain the stable transfected cells. Desired gene disruption was confirmed by Western blotting analysis of target proteins.

Western blotting

Whole-cell lysates were prepared with cell lysis buffer (Beyotime Biotechnology) and equal protein content was loaded to polyacrylamide gel electrophoresis and transferred onto polyvinylidene difluoride membranes. Next, the membranes were blocked in 5% nonfat milk in tris buffered saline with Tween 20 (TBST) for 1 hour at room temperature before incubation with antibodies. Subsequently, the membranes were incubated overnight at 4°C with the appropriate primary antibodies at a dilution of 1:1000. After incubation with fluorescein-conjugated secondary antibody at a dilution of 1:10,000 for 1 hour at room temperature, imaging of blots was performed using an Odyssey fluorescence scanner (Li-Cor, Lincoln, NE, USA). To quantify the relative protein expression, all band intensities were normalized to β-actin or the respective control proteins. Three independent substrates were run for each blot and each group.

Quantitative real-time PCR

Total RNA was extracted using TRIzol reagent (Invitrogen) and reversely transcribed into cDNA with random primers using Super-Script III reverse transcriptase (Invitrogen). Then, the resulting cDNA was used as a template for the amplification of target gene transcripts by quantitative real-time polymerase chain reaction (qRT-PCR). qRT-PCR amplification was performed in a 10-μl reaction containing SYBR Green PCR Master Mix (Applied Biosystems) on ABI PRISM 7300HT Sequence Detection System (Applied Biosystems). β-Actin was used as a control for normalization.

Flow cytometric analysis

Mice tumors were harvested, mechanically minced, and digested in collagenase IV (2 mg/ml, Sigma-Aldrich) and DNase I (50 μg/ml, Sigma-Aldrich) for 30 min at 37°C with shaking. Then, the dissociated cells were filtered through a 70-μm cell strainer and the resulting single-cell suspensions were incubated with Fc block followed by staining with the indicated surface antibodies for 30 min at 4°C. For intracellular staining, single-cell suspensions from tumors were stimulated with a cell activation cocktail (BioLegend) with protein transport inhibitor monensin (BioLegend) before surface staining. Next, cells were fixed and permeabilized with a Cyto-Fast Fix/Perm buffer set (BioLegend) for intracellular staining. Flow cytometric analysis was performed on the LSRFortessa flow cytometer (BD Biosciences) and data were analyzed by FlowJo software.

Immunofluorescence staining

Cells were plated on 35-mm poly-D-lysine–coated glass bottom dishes and fixed in 4% paraformaldehyde for 20 min. Next, cells were permeabilized with 0.1% Triton X-100 for 30 min and blocked with 4% sheep serum in phosphate-buffered saline for 1 hour at room temperature. Then, cells were incubated with primary antibodies against dsDNA and Hsp60 overnight at 4°C followed by fluorescent secondary antibodies at room temperature for 1 hour. 4′,6-Diamidino-2-phenylindole (DAPI) was used for nuclear staining. Immunofluorescence images were taken using a confocal fluorescence microscope (Olympus, Heidelberg, Germany).

OCR measurement

Seahorse XF Cell Mito Stress Test assay was conducted to measure OCR in an XF24 Extracellular Flux Analyzer (Agilent) according to the assay manual. Briefly, cells were seeded on XF24 cell culture plates and incubated for 24 hours in a humidified 37°C incubator with 5% CO_2. Before starting, the growth medium was replaced with an assay medium. The assay medium was prepared by supplementing Seahorse XF Base Medium (Agilent) with 1 mM pyruvate, 2 mM glutamine, and 20 mM glucose and adjusted to pH 7.4.

Cell proliferation and colony formation assay

Cell Counting Kit-8 (CCK8) (Vazyme) was used to detect cell proliferation. Cells were seeded in a 96-well plate at a density of 3000 cells per well. CCK-8 solution was added to each well after respective culture time of 24, 48, and 72 hours. Cell proliferation was assessed by measuring the absorbance at 450 nm using a microplate reader (Bio-Rad Laboratories). For colony formation assay, cells were seeded on a six-well plate at a density of 3000 cells per well for 2 weeks. Then, cell colonies were fixed with 4% paraformaldehyde for 20 min and stained with 1% crystal violet for 30 min. The colonies were imaged using an IX70 microscope (Olympus, Heidelberg, Germany).

IHC staining

IHC staining was performed on formalin-fixed and paraffin-embedded tissues from human HCC using the indicated antibodies via the Leica automated staining platform. The primary antibodies were used at the indicated concentrations: anti-ACLY (1:200; Abcam), anti-cGAS (1:100; Santa Cruz Biotechnology), αPD-L1 (1:200; Proteintech), and anti-CD8 (1:100; Abcam). On the basis of the immunoreactive score method, the intensity of human HCC tissue microarray staining (protein expression) was scored as 0 (negative), 1 (weak), 2 (moderate), and 3 (strong). The patients were subdivided into two groups: the low expression group (negative or weak staining) and the high expression group (moderate or strong staining) according to the immunoreactive score.

cGAMP, MDA, and PUFA measurements

cGAMP levels in cell lysates were measured using a 2′3′-cGAMP ELISA Kit (Cayman) according to the manufacturer's protocol. For sample preparation, cells were lysed in M-PER Mammalian Protein Extraction Reagent (Thermo Fisher Scientific). For the measurement of MDA levels in cell lysates, the MDA ELISA Kit (FineTest) was used according to the manufacturer's instructions. For sample preparation, cells were lysed in radioimmunoprecipitation assay buffer (Beyotime Biotechnology) and the total protein concentration was determined by the BCA Protein Assay Kit (Thermo Fisher Scientific). For measurement of intracellular PUFA levels, ARA ELISA Kit (Elabscience) and EPA ELISA Kit (Biorbyt) were used according to the manufacturer's instructions.

ACLY activity and acetyl-CoA measurements

For cellular ACLY activity measurement, an ACLY activity assay kit (Solarbio) was used according to the manufacturer's protocols. The intracellular acetyl-CoA level was measured using the PicoProbe acetyl-CoA assay kit (BioVision) according to the manufacturer's instructions.

Online database analysis

GSEA and KEGG pathway analysis in pancreatic cancer from the TCGA dataset was performed in the LinkedOmics platform (59). R2 genomics analysis and visualization platform (https://hgserver1.amc.nl/cgi-bin/r2/main.cgi) was used to evaluate the Pearson's correlation between ACLY and T cell immune checkpoint molecules or ISGs in HCC, PDAC, and melanoma datasets. Analysis of survival in patients with HCC, HNSSC, and breast cancer according to the expression of ACLY in the group with decreased or enriched intratumoral CD8^{+} T cell infiltration was conducted using an online database Kaplan-Meier plotter (60).

Statistical analysis

Statistical analysis was performed using GraphPad Prism 8 software (GraphPad Software, San Diego, CA). Data are shown as means ± SD unless stated otherwise. The specific statistical tests applied are given in the respective figure legends, where statistical significance is given by $*P < 0.05$, $**P < 0.01$, and $***P < 0.001$; n.s., not significant.

Supplementary Materials

This PDF file includes:
Figs. S1 to S6

REFERENCES AND NOTES

1. E. B. Garon, N. A. Rizvi, R. Hui, N. Leighl, A. S. Balmanoukian, J. P. Eder, A. Patnaik, C. Aggarwal, M. Gubens, L. Horn, E. Carcereny, M.-J. Ahn, E. Felip, J.-S. Lee, M. D. Hellmann, O. Hamid, J. W. Goldman, J.-C. Soria, M. Dolled-Filhart, R. Z. Rutledge, J. Zhang, J. K. Lunceford, R. Rangwala, G. M. Lubiniecki, C. Roach, K. Emancipator, L. Gandhi; KEYNOTE-001 Investigators, Pembrolizumab for the treatment of non-small-cell lung cancer. *N. Engl. J. Med.* **372**, 2018–2028 (2015).

2. C. Robert, J. Schachter, G. V. Long, A. Arance, J. J. Grob, L. Mortier, A. Daud, M. S. Carlino, C. McNeil, M. Lotem, J. Larkin, P. Lorigan, B. Neyns, C. U. Blank, O. Hamid, C. Mateus, R. Shapira-Frommer, M. Kosh, H. Zhou, N. Ibrahim, S. Ebbinghaus, A. Ribas; KEYNOTE-006 Investigators, Pembrolizumab versus ipilimumab in advanced melanoma. *N. Engl. J. Med.* **372**, 2521–2532 (2015).

3. T. Powles, J. P. Eder, G. D. Fine, F. S. Braiteh, Y. Loriot, C. Cruz, J. Bellmunt, H. A. Burris, D. P. Petrylak, S. L. Teng, X. Shen, Z. Boyd, P. S. Hegde, D. S. Chen, N. J. Vogelzang, MPDL3280A (anti–PD-L1) treatment leads to clinical activity in metastatic bladder cancer. *Nature* **515**, 558–562 (2014).

4. K. C. Ohaegbulam, A. Assal, E. Lazar-Molnar, Y. Yao, X. Zang, Human cancer immunotherapy with antibodies to the PD-1 and PD-L1 pathway. *Trends Mol. Med.* **21**, 24–33 (2015).

5. G. Morad, B. A. Helmink, P. Sharma, J. A. Wargo, Hallmarks of response, resistance, and toxicity to immune checkpoint blockade. *Cell* **184**, 5309–5337 (2021).

6. A. J. Schoenfeld, M. D. Hellmann, Acquired resistance to immune checkpoint inhibitors. *Cancer Cell* **37**, 443–455 (2020).

7. S. Zhu, T. Zhang, L. Zheng, H. Liu, W. Song, D. Liu, Z. Li, C.-X. Pan, Combination strategies to maximize the benefits of cancer immunotherapy. *J. Hematol. Oncol.* **14**, 156 (2021).

8. J. E. Bader, K. Voss, J. C. Rathmell, Targeting metabolism to improve the tumor microenvironment for cancer immunotherapy. *Mol. Cell* **78**, 1019–1033 (2020).

9. K.-C. Kao, S. Vilbois, C.-H. Tsai, P.-C. Ho, Metabolic communication in the tumour-immune microenvironment. *Nat. Cell Biol.* **24**, 1574–1583 (2022).

10. H. Lv, G. Lv, C. Chen, Q. Zong, G. Jiang, D. Ye, X. Cui, Y. He, W. Xiang, Q. Han, L. Tang, W. Yang, H. Wang, NAD(+) metabolism maintains inducible PD-L1 expression to drive tumor immune evasion. *Cell Metab.* **33**, 110–127.e5 (2021).

11. J. A. Menendez, R. Lupu, Fatty acid synthase and the lipogenic phenotype in cancer pathogenesis. *Nat. Rev. Cancer* **7**, 763–777 (2007).

12. M. Martin-Perez, U. Urdiroz-Urricelqui, C. Bigas, S. A. Benitah, The role of lipids in cancer progression and metastasis. *Cell Metab.* **34**, 1675–1699 (2022).

13. P. Icard, Z. Wu, L. Fournel, A. Coquerel, H. Lincet, M. Alifano, ATP citrate lyase: A central metabolic enzyme in cancer. *Cancer Lett.* **471**, 125–134 (2020).

14. G. Hatzivassiliou, F. Zhao, D. E. Bauer, C. Andreadis, A. N. Shaw, D. Dhanak, S. R. Hingorani, D. A. Tuveson, C. B. Thompson, ATP citrate lyase inhibition can suppress tumor cell growth. *Cancer Cell* **8**, 311–321 (2005).

15. R. Lin, R. Tao, X. Gao, T. Li, X. Zhou, K.-L. Guan, Y. Xiong, Q.-Y. Lei, Acetylation stabilizes ATP-citrate lyase to promote lipid biosynthesis and tumor growth. *Mol. Cell* **51**, 506–518 (2013).

16. A. Carrer, S. Trefely, S. Zhao, S. L. Campbell, R. J. Norgard, K. C. Schultz, S. Sidoli, J. L. D. Parris, H. C. Affronti, S. Sivanand, S. Egolf, Y. Sela, M. Trizzino, A. Gardini, B. A. Garcia, N. W. Snyder, B. Z. Stanger, K. E. Wellen, Acetyl-CoA metabolism supports multistep pancreatic tumorigenesis. *Cancer Discov.* **9**, 416–435 (2019).

17. L. Gu, Y. Zhu, X. Lin, B. Lu, X. Zhou, F. Zhou, Q. Zhao, E. V. Prochownik, Y. Li, The IKKβ-USP30-ACLY axis controls lipogenesis and tumorigenesis. *Hepatology* **73**, 160–174 (2021).

18. K. K. Ray, H. E. Bays, A. L. Catapano, N. D. Lalwani, L. T. Bloedon, L. R. Sterling, P. L. Robinson, C. M. Ballantyne; CLEAR Harmony Trial, C. H. Trial, Safety and efficacy of bempedoic acid to reduce LDL cholesterol. *N. Engl. J. Med.* **380**, 1022–1032 (2019).

19. K.-P. Hopfner, V. Hornung, Molecular mechanisms and cellular functions of cGAS-STING signalling. *Nat. Rev. Mol. Cell Bio.* **21**, 501–521 (2020).

20. X. Zhang, X.-C. Bai, Z. J. Chen, Structures and mechanisms in the cGAS-STING innate immunity pathway. *Immunity* **53**, 43–53 (2020).

21. J. Kwon, S. F. Bakhoum, The cytosolic DNA-sensing cGAS-STING pathway in cancer. *Cancer Discov.* **10**, 26–39 (2020).

22. A. Amouzegar, M. Chelvanambi, J. N. Filderman, W. J. Storkus, J. J. Luke, STING agonists as cancer therapeutics. *Cancers* **13**, 2695 (2021).

23. F. Meric-Bernstam, R. F. Sweis, F. S. Hodi, W. A. Messersmith, R. H. I. Andtbacka, M. Ingham, N. Lewis, X. Chen, M. Pelletier, X. Chen, J. Wu, S. M. McWhirter, T. Müller, N. Nair, J. J. Luke, Phase I dose-escalation trial of MIW815 (ADU-S100), an intratumoral STING agonist, in patients with advanced/metastatic solid tumors or lymphomas. *Clin. Cancer Res.* **28**, 677–688 (2022).

24. N. Samson, A. Ablasser, The cGAS-STING pathway and cancer. *Nat. Cancer* **3**, 1452–1463 (2022).

25. A. N. Cheng, L. C. Cheng, C. L. Kuo, Y. K. Lo, H. Y. Chou, C. H. Chen, Y. H. Wang, T. H. Chuang, S. J. Cheng, A. Y. Lee, Mitochondrial Lon-induced mtDNA leakage contributes to PD-L1-

mediated immunoescape via STING-IFN signaling and extracellular vesicles. *J. Immunother. Cancer* **8**, e001372 (2020).

26. D. B. Doroshow, S. Bhalla, M. B. Beasley, L. M. Sholl, K. M. Kerr, S. Gnjatic, I. I. Wistuba, D. L. Rimm, M. S. Tsao, F. R. Hirsch, PD-L1 as a biomarker of response to immune-checkpoint inhibitors. *Nat. Rev. Clin. Oncol.* **18**, 345–362 (2021).

27. A. Li, M. Yi, S. Qin, Y. Song, Q. Chu, K. Wu, Activating cGAS-STING pathway for the optimal effect of cancer immunotherapy. *J. Hematol. Oncol.* **12**, 35 (2019).

28. M. Lv, M. Chen, R. Zhang, W. Zhang, C. Wang, Y. Zhang, X. Wei, Y. Guan, J. Liu, K. Feng, M. Jing, X. Wang, Y. C. Liu, Q. Mei, W. Han, Z. Jiang, Manganese is critical for antitumor immune responses via cGAS-STING and improves the efficacy of clinical immunotherapy. *Cell Res.* **30**, 966–979 (2020).

29. J. M. Llovet, R. K. Kelley, A. Villanueva, A. G. Singal, E. Pikarsky, S. Roayaie, R. Lencioni, K. Koike, J. Zucman-Rossi, R. S. Finn, Hepatocellular carcinoma. *Nat. Rev. Dis. Primers* **7**, 6 (2021).

30. N. J. Pearce, J. W. Yates, T. A. Berkhout, B. Jackson, D. Tew, H. Boyd, P. Camilleri, P. Sweeney, A. D. Gribble, A. Shaw, P. H. Groot, The role of ATP citrate-lyase in the metabolic regulation of plasma lipids. Hypolipidaemic effects of SB-204990, a lactone prodrug of the potent ATP citrate-lyase inhibitor SB-201076. *Biochem. J.* **334** (Pt. 1), 113–119 (1998).

31. M. J. White, K. McArthur, D. Metcalf, R. M. Lane, J. C. Cambier, M. J. Herold, M. F. van Delft, S. Bedoui, G. Lessene, M. E. Ritchie, D. C. Huang, B. T. Kile, Apoptotic caspases suppress mtDNA-induced STING-mediated type I IFN production. *Cell* **159**, 1549–1562 (2014).

32. E. Rysman, K. Brusselmans, K. Scheys, L. Timmermans, R. Derua, S. Munck, P. P. Van Veldhoven, D. Waltregny, V. W. Daniëls, J. Machiels, F. Vanderhoydonc, K. Smans, E. Waelkens, G. Verhoeven, J. V. Swinnen, De novo lipogenesis protects cancer cells from free radicals and chemotherapeutics by promoting membrane lipid saturation. *Cancer Res.* **70**, 8117–8126 (2010).

33. H. Yin, L. Xu, N. A. Porter, Free radical lipid peroxidation: Mechanisms and analysis. *Chem. Rev.* **111**, 5944–5972 (2011).

34. D. Tsikas, Assessment of lipid peroxidation by measuring malondialdehyde (MDA) and relatives in biological samples: Analytical and biological challenges. *Anal. Biochem.* **524**, 13–30 (2017).

35. C. M. Harmon, N. A. Abumrad, Binding of sulfosuccinimidyl fatty acids to adipocyte membrane proteins: Isolation and amino-terminal sequence of an 88-kD protein implicated in transport of long-chain fatty acids. *J. Membr. Biol.* **133**, 43–49 (1993).

36. H. Wang, S. Hu, X. Chen, H. Shi, C. Chen, L. Sun, Z. J. Chen, cGAS is essential for the antitumor effect of immune checkpoint blockade. *Proc. Natl. Acad. Sci. U.S.A.* **114**, 1637–1642 (2017).

37. L. Chen, L. Diao, Y. Yang, X. Yi, B. L. Rodriguez, Y. Li, P. A. Villalobos, T. Cascone, X. Liu, L. Tan, P. L. Lorenzi, A. Huang, Q. Zhao, D. Peng, J. J. Fradette, D. H. Peng, C. Ungewiss, J. Roybal, P. Tong, J. Oba, F. Skoulidis, W. Peng, B. W. Carter, C. M. Gay, Y. Fan, C. A. Class, J. Zhu, J. Rodriguez-Canales, M. Kawakami, L. A. Byers, S. E. Woodman, V. A. Papadimitrakopoulou, E. Dmitrovsky, J. Wang, S. E. Ullrich, I. I. Wistuba, J. V. Heymach, F. X.-F. Qin, D. L. Gibbons, CD38-mediated immunosuppression as a mechanism of tumor cell escape from PD-1/PD-L1 blockade. *Cancer Discov.* **8**, 1156–1175 (2018).

38. S. L. Pinkosky, S. Filippov, R. A. Srivastava, J. C. Hanselman, C. D. Bradshaw, T. R. Hurley, C. T. Cramer, M. A. Spahr, A. F. Brant, J. L. Houghton, C. Baker, M. Naples, K. Adeli, R. S. Newton, AMP-activated protein kinase and ATP-citrate lyase are two distinct molecular targets for ETC-1002, a novel small molecule regulator of lipid and carbohydrate metabolism. *J. Lipid Res.* **54**, 134–151 (2013).

39. E. Dierge, Y. Larondelle, O. Feron, Cancer diets for cancer patients: Lessons from mouse studies and new insights from the study of fatty acid metabolism in tumors. *Biochimie* **178**, 56–68 (2020).

40. N. Mabrouk, B. Lecoeur, A. Bettaieb, C. Paul, F. Végran, Impact of lipid metabolism on antitumor immune response. *Cancers* **14**, 1850 (2022).

41. D. L. Herber, W. Cao, Y. Nefedova, S. V. Novitskiy, S. Nagaraj, V. A. Tyurin, A. Corzo, H. I. Cho, E. Celis, B. Lennox, S. C. Knight, T. Padhya, T. V. McCaffrey, J. C. McCaffrey, S. Antonia, M. Fishman, R. L. Ferris, V. E. Kagan, D. I. Gabrilovich, Lipid accumulation and dendritic cell dysfunction in cancer. *Nat. Med.* **16**, 880–886 (2010).

42. H. Wu, Y. Han, Y. Rodriguez Sillke, H. Deng, S. Siddiqui, C. Treese, F. Schmidt, M. Friedrich, J. Keye, J. Wan, Y. Qin, A. A. Kühl, Z. Qin, B. Siegmund, R. Glauben, Lipid droplet-dependent fatty acid metabolism controls the immune suppressive phenotype of tumor-associated macrophages. *EMBO Mol. Med.* **11**, e10698 (2019).

43. M. Song, X. Zhang, J. A. Meyerhardt, E. L. Giovannucci, S. Ogino, C. S. Fuchs, A. T. Chan, Marine ω-3 polyunsaturated fatty acid intake and survival after colorectal cancer diagnosis. *Gut* **66**, 1790–1796 (2017).

44. E. L. Van Blarigan, C. S. Fuchs, D. Niedzwiecki, X. Ye, S. Zhang, M. Song, L. B. Saltz, R. J. Mayer, R. B. Mowat, R. Whittom, A. Hantel, A. Benson, D. Atienza, M. Messino, H. Kindler, A. Venook, S. Ogino, E. L. Giovannucci, J. A. Meyerhardt, Marine ω-3 polyunsaturated fatty acid and fish intake after colon cancer diagnosis and survival: CALGB 89803 (Alliance). *Cancer Epidemiol. Biomarkers Prev.* **27**, 438–445 (2018).

45. M. A. Perez, L. Magtanong, S. J. Dixon, J. L. Watts, Dietary lipids induce ferroptosis in *Caenorhabditis elegans* and human cancer cells. *Dev. Cell* **54**, 447–454.e4 (2020).

46. E. Dierge, E. Debock, C. Guilbaud, C. Corbet, E. Mignolet, L. Mignard, E. Bastien, C. Dessy, Y. Larondelle, O. Feron, Peroxidation of n-3 and n-6 polyunsaturated fatty acids in the acidic tumor environment leads to ferroptosis-mediated anticancer effects. *Cell Metab.* **33**, 1701–1715.e5 (2021).

47. X. Chen, Y. Liu, Y. Wang, C. Wang, X. Chen, Y. Xiong, L. Liu, X. Yuan, H. Tang, C. Shu, J. Zhang, A. M. Guo, H. Chen, J. Yang, CYP4F2-catalyzed metabolism of arachidonic acid promotes stromal cell-mediated immunosuppression in non-small cell lung cancer. *Cancer Res.* **82**, 4016–4030 (2022).

48. R. B. Zurier, Fatty acids, inflammation and immune responses. *Prostaglandins Leukot. Essent. Fatty Acids* **48**, 57–62 (1993).

49. C. B. Nava Lauson, S. Tiberti, P. A. Corsetto, F. Conte, P. Tyagi, M. Machwirth, S. Ebert, A. Loffreda, L. Scheller, D. Sheta, Z. Mokhtari, T. Peters, A. T. Raman, F. Greco, A. M. Rizzo, A. Beilhack, G. Signore, N. Tumino, P. Vacca, L. A. McDonnell, A. Raimondi, P. D. Greenberg, J. B. Huppa, S. Cardaci, I. Caruana, S. Rodighiero, L. Nezi, T. Manzo, Linoleic acid potentiates CD8+ T cell metabolic fitness and antitumor immunity. *Cell Metab.* **35**, 633–650.e9 (2023).

50. P. Liao, W. Wang, W. Wang, I. Kryczek, X. Li, Y. Bian, A. Sell, S. Wei, S. Grove, J. K. Johnson, P. D. Kennedy, M. Gijón, Y. M. Shah, W. Zou, CD8+ T cells and fatty acids orchestrate tumor ferroptosis and immunity via ACSL4. *Cancer Cell* **40**, 365–378.e6 (2022).

51. T. Sen, B. L. Rodriguez, L. Chen, C. M. D. Corte, N. Morikawa, J. Fujimoto, S. Cristea, T. Nguyen, L. Diao, L. Li, Y. Fan, Y. Yang, J. Wang, B. S. Glisson, I. I. Wistuba, J. Sage, J. V. Heymach, D. L. Gibbons, L. A. Byers, Targeting DNA damage response promotes antitumor immunity through STING-mediated T-cell activation in small cell lung cancer. *Cancer Discov.* **9**, 646–661 (2019).

52. R. M. Chabanon, G. Muirhead, D. B. Krastev, J. Adam, D. Morel, M. Garrido, A. Lamb, C. Hénon, N. Dorvault, M. Rouanne, R. Marlow, I. Bajrami, M. L. Cardeñosa, A. Konde, B. Besse, A. Ashworth, S. J. Pettitt, S. Haider, A. Marabelle, A. N. Tutt, J. C. Soria, C. J. Lord, S. Postel-Vinay, PARP inhibition enhances tumor cell-intrinsic immunity in ERCC1-deficient non-small cell lung cancer. *J. Clin. Invest.* **129**, 1211–1228 (2019).

53. T. Reisländer, F. J. Groelly, M. Tarsounas, DNA damage and cancer immunotherapy: A STING in the tale. *Mol. Cell* **80**, 21–28 (2020).

54. S. Grabosch, M. Bulatovic, F. Zeng, T. Ma, L. Zhang, M. Ross, J. Brozick, Y. Fang, G. Tseng, E. Kim, A. Gambotto, E. Elishaev, R. P. Edwards, A. M. Vlad, Cisplatin-induced immune modulation in ovarian cancer mouse models with distinct inflammation profiles. *Oncogene* **38**, 2380–2393 (2019).

55. C. Zierhut, N. Yamaguchi, M. Paredes, J. D. Luo, T. Carroll, H. Funabiki, The cytoplasmic DNA Sensor cGAS promotes mitotic cell death. *Cell* **178**, 302–315.e23 (2019).

56. T. B. Steinbichler, J. Dudás, S. Skvortsov, U. Ganswindt, H. Riechelmann, Therapy resistance mediated by cancer stem cells. *Semin. Cancer Biol.* **53**, 156–167 (2018).

57. Q. Han, C. A. Chen, W. Yang, D. Liang, H. W. Lv, G. S. Lv, Q. N. Zong, H. Y. Wang, ATP-citrate lyase regulates stemness and metastasis in hepatocellular carcinoma via the Wnt/β-catenin signaling pathway. *Hepatobiliary Pancreat. Dis. Int.* **20**, 251–261 (2021).

58. A. Husain, Y. T. Chiu, K. M. Sze, D. W. Ho, Y. M. Tsui, E. M. S. Suarez, V. X. Zhang, L. K. Chan, E. Lee, J. M. Lee, T. T. Cheung, C. C. Wong, C. Y. Chung, I. O. Ng, Ephrin-A3/EphA2 axis regulates cellular metabolic plasticity to enhance cancer stemness in hypoxic hepatocellular carcinoma. *J. Hepatol.* **77**, 383–396 (2022).

59. S. V. Vasaikar, P. Straub, J. Wang, B. Zhang, LinkedOmics: Analyzing multi-omics data within and across 32 cancer types. *Nucleic Acids Res.* **46**, D956–d963 (2018).

60. A. Lánczky, B. Győrffy, Web-based survival analysis tool tailored for medical research (KMplot): Development and implementation. *J. Med. Internet Res.* **23**, e27633 (2021).